Circulating exosomal microRNA as potential biomarkers of hepatic injury and inflammation inGlycogen Storage Disease type 1a

Roberta Resaz[1#], Davide Cangelosi[1#], Martina Morini[1], Daniela Segalerba[1],Luca Mastracci[2,3], Federica Grillo[2,3], Maria Carla Bosco[1], Cristina Bottino[4,5], Irma Colombo[6] and Alessandra Eva[1§]

1. Laboratory of MolecularBiology, IRCCS Istituto Giannina Gaslini, Via G. Gaslini 5, 16147 Genova, Italy

2. Department of Surgical and Diagnostic Sciences (DISC), Anatomic Pathology Unit, Università degli studi di Genova, Viale Benedetto XV 6, 16132 Genova, Italy

3. National Cancer Research Institute, IRCCS Ospedale Policlinico San Martino, Largo Rosanna Benzi 10, 16132 Genova, Italy

4. Department of Experimental Medicine, School of Medicine, Università degli Studi di Genova, Italy

5. Laboratory of Clinical and Experimental Immunology. IRCCS Istituto Giannina Gaslini, Via G. Gaslini 5, 16147 Genova, Italy

6.Department of Pharmacological and Biomolecular Sciences, Università degli Studi di Milano, via D. Trentacoste 2, 20134 Milano, Italy

#. These authors contributed equally to this work.

§. Corresponding author.

Corresponding author

Alessandra Eva

Laboratory of Molecular Biology

IRCCS Istituto Giannina Gaslini

Via Gerolamo Gaslini 5, 16147 Genova

Tel.: +39 010 56363545

Fax.: +39 010 3733346

Email: alessandraeva@gaslini.org

Disease Models & Mechanisms • DMM • Accepted manuscript

Financial support

This work was supported by grants from Associazione Italiana Ricerca sul Cancro (AIRC 2014 Grant IG15461 to A.E.), from Associazione Italiana Glicogenosi (to A. E.), from Compagnia di San Paolo (Grant 318 to A.E.), and from the Italian Ministry of Health (Ricerca Corrente).

Acknowledgement

This work was supported by grants from Associazione Italiana Ricerca sul Cancro (AIRC 2014 Grant IG15461 to A.E.), from Associazione Italiana Glicogenosi (to A.E.), from Compagnia di San Paolo (Grant 318 to A.E.) and from the Italian Ministry of Health (Ricerca Corrente).

The support and encouragement of the Associazione Italiana Glicogenosi was instrumental and essential for the execution of the present work.

Declarations of interest: none

ABSTRACT

Most patients affected by Glycogen storage disease type 1a (GSD-1a), an inherited metabolic disorder caused by mutations in the enzyme glucose-6-phosphatase-alpha (G6Pase-α), develop renal and liver complications, including development of hepatocellular adenoma/carcinoma. The purpose of this study was to identify potential biomarkers of the pathophysiology of the GSD1a affected liver. To this end, we utilized the plasma exosomes of a murine model of GSD-1a, LS-G6pc$^{-/-}$ mice, to uncover microRNA expression modulation associated with the disease. Differentially expressed microRNA between LS-G6pc$^{-/-}$ and wild type mice, LS-G6pc$^{-/-}$ mice with hepatocellular adenoma and LS-G6pc$^{-/-}$ mice without adenoma, and LS-G6pc$^{-/-}$ mice with amyloidosis and LS-G6pc$^{-/-}$ mice without amyloidosis were identified. Pathway analysis demonstrated that the target genes of the differentially expressed microRNA were significantly enriched for insulin signaling pathway, glucose and lipid metabolism, Wnt-beta catenin, telomere maintenance and hepatocellular carcinoma, and chemokine and immune regulation signaling pathways. While some microRNA were common to the different pathologic conditions others were unique to cancerous or inflammatory status of the animals. Therefore, the altered expression of several microRNA correlates with various pathologic liver statuses and may help discriminate during the progression of the disease and the development of late GSD1-a associated complications.

INTRODUCTION

GSD1a is an autosomal rare metabolic disorder caused by a mutation in the catalytic subunit of glucose-6-phosphatase-α (G6Pase-α), a key enzyme in glucose homeostasis. G6Pase-α is expressed in the liver, kidney and intestine, and catalyzes the hydrolysis of glucose-6-phosphate (G6P) to glucose and phosphate, the terminal steps in gluconeogenesis and glycogenolysis (Chou et al. 2002).

GSD1apatients are unable to maintain glucose homeostasis and show growth retardation, hypoglycemia, hepatomegaly, kidney enlargement, hyperlipidemia, hyperuricemia, and lactic acidemia. Long-term symptoms include gout, osteoporosis, renal failure, and hepatic adenomas with risk for malignancy. The disease is controlled by dietary therapies, which consist of continuous nasogastric infusion of glucose or frequent oral administration of uncooked cornstarch (Chen et al. 1984), to prevent hypoglycemia.

Unfortunately, the control of hypoglycemia cannot prevent the progressive deterioration of liver and kidney. Liver dysmetabolism is severe and the hematochemical parameters are altered with high triglycerides and cholesterol content. Persistency of liver dysmetabolism results in a progressive worsening of the clinical parameters, and the formation of hepatocellular adenomas (HCA), which may progress to hepatocellular carcinoma (HCC) in 10% of the cases (Labrune et al. 1997). 52% of GSD adenomas can be classified as inflammatory type (IHCA), 28% as β-catenin-mutated type with upregulation of glutamine synthetase (bHCA), and the remaining 20% as unclassified (UHCA) (Calderaro et al. 2013). The elevated percentage of adenomas with β-catenin activating mutations may explain the risk of malignant transformation of HCA in HCC in GSD1a patients. Liver transplant is the only option in the most severe cases.

GSD1a patients exhibit marked variability in the severity of symptoms and complications, and the underlying pathological pathways that develop with the progress of the disease are poorly understood. microRNA are small non-coding RNA that regulate gene expression by targeting messenger RNA and are actively studied as biomarkers for their stability, as diagnostic/prognostic indicators for their mirroring

cellular components, and as a source of indication of therapeutic targets for their biological activities. Aberrant microRNA expression profiles were reported in cancer, rare diseases, and tissue degeneration (Hu et al. 2012).

The utilization of genetically engineered mouse models can be an efficient mean of discovering prognostic markers and can minimize the problems associated with the use of human subjects, such as the variability in the histopathological subtypes of the subjects enrolled in the study, or the lack of homogeneous methods for sample collection and storage, because we can control the age of the mice, the environmental factors, and the sampling protocol.

In this study, we explored the possibility to use exosomal microRNA (Exo-miR) as disease markers in a liver-specific murine model of GSD1a,LS-G6pc$^{-/-}$, we have generated (Resaz et al. 2014). Our animal model, in which only the liver is affected, is ideal to identify exosomal microRNA contribution to the specific GSD1a hepatic pathologic manifestations. We analyzed the expression of Exo-miR in the plasma of LS-G6pc$^{-/-}$ mice, to derive specific biomarkers and prognostic indicators of liver degeneration, HCA onset, and its progression to HCC. We identified potential biomarkers of the pathophysiology of the diseased liver, including Exo-miR discriminating LS-G6pc$^{-/-}$ mice with adenomas versus LS-G6pc$^{-/-}$ mice without adenomas. Our results indicate the potential of blood as a surrogate tissue to study HCA development and HCC malignant transformation in GSD1a patients.

MATERIALS AND METHOD

Sample collection, histology, and phenotype analyses

All animals were maintained in a conventional animal facility in 12-h light/dark cycles, fed at libitum, and monitored for their lifespan. All animal studies were approved by the Ethical Committee for Animal Experimentation (CSEA) as Animal Use project n. 291 communicated to the Italian Ministry of Health having regard to the article of the D.lgs 116/92, and carried out at the animal facility of the National Institute for Cancer Research (Genova, Italy). Livers were fixed in 10% buffered formalin for 24 hours. Formalin fixed tissues were then processed and four micrometer thick sections were cut and stained with haematoxylin and eosin for histological analysis. All animals were

phenotypically evaluated as described (Resaz, et al. 2014). Sixteen LS-G6pc$^{-/-}$ mice developed hepatic adenoma. Livers of WT mice were normal.

Exosome isolation and microRNA purification from plasma

Blood was collected at the time of the sacrifice from the left ventricle with a syringe in EDTA tubes and centrifuged at 2100 rpm for 10 minutes at room temperature (RT) to collect plasma. Plasma was stored at -80° C to be used for exosome isolation. Samples were collected at different time-points (1-3, 4-6, 7-9, 10-12, and 13-15 months) that reflect different stages of disease progression. Exosomes isolation and RNA extraction was performed with the exoRNeasy Serum/Plasma Midi kit (Qiagen Italia, Milano, Italy), as recommended by the manufacturer. Briefly, to isolate exosomes, 100 µl of plasma were centrifuged at 16,000 x g at 4°C to eliminate cellular debris. Supernatants were then mixed with one volume of XBP binding buffer, loaded onto the exoEasy spin column, and spun at 500 x g 1 minute at RT. Exosomes, bound to the filter of the column, were washed with 3.5 ml of XWP Washing Buffer by centrifuging at 5,000 x g for 5 minutes at RT. The spin column was transferred to a new collection tube and centrifuged at 5,000 x g for 5 minutes at RT after the addition of 700 µl of QIAzol to the membrane, to lyse exosomes and proceed with RNA purification. RNA extraction was performed according to the manufacturer's instructions. Quality control evaluation was performed with the Agilent 2100 Bioanalyzer, using the Small RNA Assay (Agilent Technologies Spa, Cernusco sul Naviglio, Milano, Italy).

Quantitative Real Time PCR (qRT-PCR)

Exo-miRwere analyzed by the TaqMan Array Card Technology. Exo-miR were reverse transcribed with the TaqMan® microRNA Reverse Transcription Kit, using the Megaplex^{TM}RT primers Rodent Pool A (Thermo Fisher Scientific, Monza, MB, Italy). Pre-amplification of cDNA was performed with TaqMan®PreAmp Master Mix and Megaplex^{TM}Pre-Amp primers Rodent Pool A. The pre-amplification product was diluted according to the manufacturer's instructions and used to perform microRNA profiling on the ViiATM 7 Real-Time PCR System. Briefly, 9 µl of the diluted pre-amplified product was mixed with 450 µl TaqMan® Universal Master Mix II, No UNG

(Thermo Fisher Scientific, Monza, MB, Italy) and 441 µl of nuclease-free water. 100 µl of the PCR reaction mix was dispensed into each well of the TaqMan® Array Rodent microRNA A card(Thermo Fisher Scientific, Monza, MB, Italy), enabling the quantification of 381 microRNA. The Exo-miR modulation of expression in LS-G6pc$^{-/-}$ mice was validated for five microRNA by qRT-PCR on the ViiATM 7 Real-Time PCR System. Briefly, 0.3 µl of the diluted pre-amplified product was mixed with 7.5 µl TaqMan® Universal Master Mix II, No UNG (Thermo Fisher Scientific, Monza, MB, Italy), 1.75 µl of nuclease-free water, and 0.75 µl of primers specific for each microRNA. The ΔCT obtained with the Array Card was compared with that obtained by qRT-PCR to confirm microRNA differential expression in every groups analyzed.

Bioinformatic procedures and statistical analysis

Data processing, categorization, normalization, filtering, imputation and differential expression was carried out by PIPE-T galaxy tool (Zanardi et al. 2019). Ct values falling within the range 14-32 were categorized as reliable values as recommended by the manufacturer guidelines. Global mean normalization was used to reduce any technical variability introduced in the data by the RT-qPCR experiments (Zanardi et al. 2019). Only Exo-miR with at most 5% of missing values were retained for the analysis to reduce the bias introduced by imputation. Mestdagh method (Zanardi et al. 2019) was employed to assign a numeric expression value to missing values. The rank product method (Zanardi et al. 2019) implemented by RankProd R package was used to identify significant differentially expressed microRNA. Pathway analysis was performed for both predicted and validated targets of an Exo-miR using mirWalk 3.0 (Sticht et al. 2018) and carried out using gene ontology and KEGG gene set collections. An additional enrichment analysis was carried out using HALLMARK gene sets taken from MSigDB version 6.2 (Liberzon et al. 2015).The list of targets associated with an Exo-miR was identified setting up mouse as species type. For time course analysis mice were grouped according to their age into 6 groups, from 1 month to 18 months, three months apart and the analysis was carried out using BETR R package (Aryee et al. 2009). To control the expected number of false positive findings, we set up a maximum false discovery rate (FDR) of 5%. In order to focus on the most reliable age-dependent modulated Exo-miR, we considered an Exo-miR to be significant if the differential expression probability was greater than 0.7. Overlapping among the lists of genes was

carried out by Venn diagrams. Significance of the overlapping was estimated by hypergeometric statistics using Stats R package (R Core Team 2014). The degree of correlation between the CT values of RT-qPCR array cards and of validation experiments was assessed by Pearson correlation. The significance of the difference of expression between LS-G6pc$^{-/-}$ and WT mice or tumors with HCA and those without HCA in the validation experiments was calculated using unpaired t-test. Statistical analysis was carried out using GraphPad Prism version 6.0 for Mac, www.graphpad.com.

RESULTS

Analysis of Exo-miR and data normalization

We searched for Exo-miR biomarkers for GSD1a pathologic manifestations in plasma exosomes of LS-G6pc$^{-/-}$ mice at different ages by comparing the Exo-miR expression profiles of diseased versus control mice (WT).The flowchart summarizing the main steps of these analyses is shown in Supplementary Figure 1. Mice were divided into six groups according to their age. A total of 45 LS-G6pc$^{-/-}$ and 18 WT mice were analyzed. All LS-G6pc$^{-/-}$ utilized in the study displayed the features typical of this mouse model of GSD1a (Resaz et al. 2014). Sixteen LS-G6pc$^{-/-}$ mice developed HCA. None of the WT mice showed liver abnormalities, as expected. Exosomes from 100 µl of plasma of LS-G6pc$^{-/-}$mice and relative controls were isolated. Total RNA was extracted and the presence of Exo-miR was evaluated by capillary electrophoresis to ensure a sufficient retrieval of material for the following analyses. RNA samples were reverse transcribed, pre-amplified, and used to set up a rodent microRNA array card that allowed measuring the expression of 381 targets for each sample by qRT-PCR.

Raw qRT-PCR expression data were analyzed by PIPE-T tool to remove any unwanted technical variability, filtering out Exo-miR whose expression was not sufficiently reliable and handling eventual missing values occurring in the raw data profiles (see methods). The raw data were normalized using the Global Mean Method (Mestdagh et al. 2009),which was effective in reducing unwanted technical variability (Supplementary Figure 2A, 2B). Noise reduction was significant (Kolmogorov-Smirnov p value<0.05), as shown in Supplementary Figure 2C. As missing values are

not rare when microRNA expression values are analyzed, we measured their proportion in LS-G6pc$^{-/-}$ and WT profiles and found that 11769 out of 24192 Ct values (48.6%) were missing. Because missing values are difficult to handle using the standard statistical analysis, it was necessary to filter out those Exo-miR whose number of missing values exceeded 5% of the number of samples and impute the remaining missing values. We used the Mestdagh method for imputing missing values. After filtering and imputation, we obtained a total number of 61 Exo-miR to be considered for further analysis (data not shown).

LS-G6pc$^{-/-}$ mice express deregulated Exo-miR

We compared Exo-miR expression levels in groups of mice characterized by various pathological conditions to identify deregulated Exo-miR or an Exo-miR signature specific for the evolution of the disease. First, we compared LS-G6pc$^{-/-}$mice versus WT mice. Our analysis identified 11down regulated and 1 up regulated Exo-miR in LS-G6pc$^{-/-}$ mice in comparison with WT mice (Table 1).Of these, several, including miR-29amiR-145a-5p, miR-342-3p, miR-744-5pmiR-15b-5p, and miR-142-3p are considered biomarkers of HCC and involved in HCC growth, metastasis or resistance to chemotherapy (Chen et al. 2015; Fu et al. 2018; Gao et al. 2017; Li et al. 2017; Liu et al. 2018; Mahati et al. 2017; Qiu et al. 2019; Shi et al. 2015; Tan et al. 2015; Tsang et al. 2015; Wang et al. 2017).Moreover, the down-regulated miRNA let-7i-5p, miR-29-3p, miR-342-3p and miR-744-5p have been associated with signaling pathways relevant in glucose and lipid metabolism (Cheng et al. 2018; Li et al. 2013; Liang et al. 2013; Zhang et al. 2019b; Zhu et al. 2011).

We then compared Exo-miR expression levels in LS-G6pc$^{-/-}$mice with HCA versusLS-G6pc$^{-/-}$mice without HCA. Differential expression analysis by Rank Product method identified 1 downregulated and 1 up regulated Exo-miR, in LS-G6pc$^{-/-}$ mice with HCA compared with LS-G6pc$^{-/-}$ without HCA (Table 1). Of note, miR-145a-5p was found down regulated also in LS-G6pc$^{-/-}$ mice compared with WT(Table 1).

We reported that 90% of LS-G6pc$^{-/-}$mice show marked amyloid deposition in the liver and kidney by 12 months of age (Resaz et al 2014). Amyloidosis is a complication of GSD, especially 1b, usually with a renal localization (Dick et al. 2012). The reason for this is not clear but it is reasonable to speculate that amyloidosis in LS-G6pc$^{-/-}$may be associated with liver inflammation. Thus, we compared Exo-miR expression levels in LS-G6pc$^{-/-}$mice with and without amyloidosis. Differential expression analysis

identified 2 down regulated Exo-miR and 5 up regulated Exo-miR in LS-G6pc$^{-/-}$ mice with amyloidosis compared with LS-G6pc$^{-/-}$ without amyloidosis. Among these, some Exo-miR were found deregulated also in the other groups analyzed (Table 1). In fact, miR-192-5p and miR-409-3p were up regulated, and miR-486a-5p was down regulated also in LS-G6pc$^{-/-}$ mice compared with WT (Table 1).Interestingly, miR-192-5p, miR-345-5p, miR-409-3p, miR-21a-5p and miR-150-5p have been associated with an inflammatory condition, and, among them, miR-345-5p, miR-21a-5p, and miR-150-5p are unique to the amyloidosis status of the animals.

Therefore, the altered expression of several Exo-miR correlates with various pathologic liver conditions and may help discriminate affected animals during the progression of the disease and development of late GSD1a associated complications.

Time-course analysis highlights the age-dependent modulation of Exo-miR representation in LS-G6pc$^{-/-}$ mouse exosomes.

Understanding the trend of expression of candidate Exo-miR could provide an insight as to biomarker determination. Ideal biomarkers would not only be able to discriminate GSD1a patients from healthy ones, but also indicate the clinical stage. Therefore, the age dependent modulation of Exo-miR representation may be instrumental to find biomarkers of LS-G6pc$^{-/-}$mouse disease. The levels of the 61 Exo-miR were examined in LS-G6pc$^{-/-}$mice at different time points during disease progression using BETR method. The medians of their levels in both LS-G6pc$^{-/-}$and WT mice exosomes were plotted at 1-3, 4-6, 7-9, 10-12, 12-15, and 16-18 months of age. The level of expression of 14 microRNA was significantly reduced in LS-G6pc$^{-/-}$mice compared with WT mice in all age groups (Figure 1). miR-744-5p, miR-29a-3p, miR-15b-5p, miR-342-3p, and let-7i-5p were among the most significantly down regulated microRNA comparing LS-G6pc$^{-/-}$ and WT mice. Furthermore, the levels of expression of let-7d and miR-142-3p in LS-G6pc$^{-/-}$mice increased over time starting from a down regulation in younger LS-G6pc$^{-/-}$mice and becoming an up regulation in the older LS-G6pc$^{-/-}$mice. These findings indicate an age-dependent modulation of expression as LS-G6pc$^{-/-}$mice grew older.

Validation of microRNA by qPCR

To verify our findings, Exo-miR extracted from plasma of LS-G6pc$^{-/-}$ mice and WT mice were analyzed by individual qPCR based on specific TaqMan microRNA Assays. Ten different Exo-miR, differentially represented in LS-G6pc$^{-/-}$ mice in comparison with WT mice or in LS-G6pc$^{-/-}$ mice with HCA in comparison with LS-G6pc$^{-/-}$ mice without HCA, were validated. Correlation analysis was carried out by Pearson correlation and linear regression analysis between RT-qPCR and array cards Ct values to assess the reproducibility of our experiments. The results confirmed a high positive correlation of microRNA representation between the two experiments ($r>0.48$ and $p<0.05$, Supplementary Figure 3). Furthermore, we performed a differential expression analysis between LS-G6pc$^{-/-}$ mice and WT mice using an unpaired t test on the Ct values generated with array cards. Ct value was significantly higher for LS-G6pc$^{-/-}$ than WT mice, confirming the down regulation of these microRNA ($p<0.05$, Supplementary Figure 4). These results validate the data of the microRNA analysis performed.

Pathway analysis reveals the enrichment of insulin, chemokine, hypoxia, and Wnt pathways in the profile of LS-G6pc$^{-/-}$ mouse exosomes

We performed a pathway analysis based on microRNA target genes using gene ontology processes and KEGG pathways anthologies. Pathway analysis was carried out for each significant Exo-miR (Table 1) using MirWalk tool. Each significantly enriched pathway was associated with its regulating microRNA. For each set of Exo-miR, the enriched pathways and processes were collected and organized into a functional enrichment results table. For the set of Exo-miR significantly modulated in LS-G6pc$^{-/-}$ versus WT mice, MirWalk identified 8384 targets. Pathway analysis showed significant enrichment of 32 GO biological processes and 62 KEGG pathways (adjust p-value<0.05, Supplementary Table 1). Among them, we observed an enrichment of target genes associated with AMPK and insulin signaling pathway and thus with glucose and lipid metabolism for both miR744-5p and miR342-3p. Moreover, the enrichment of target genes involved in diabetes and its complications were associated with miR 744-5p.miR 342-3p and miR let-7i-5p modulate genes associated with cancer pathways and, among them, many genes linked to Wnt/beta-catenin pathway. In

addition, two microRNA targeting genes involved in chemokine signaling pathways (miR-744-5p), differentiation and activation of myeloid and lymphoid cells (let-7i-5p) were down regulated (Table 2). For the set of Exo-miR significantly modulated in LS-G6pc$^{-/-}$ with HCA versus LS-G6pc$^{-/-}$ without HCA mice, MirWalk identified 2605 targets. Pathway analysis showed significant enrichment of 34 GO biological processes and 16 KEGG pathways (adjust p-value<0.05, Supplementary Table 2). In particular, we observed an enrichment of miR-192-5p target genes involved in telomere maintenance and hepatocellular carcinoma and in the signaling pathway of FOXO1, a transcription factor that plays important roles in the regulation of gluconeogenesis and glycogenolysis by insulin signaling. Moreover, miR-192-5p targets genes involved in insulin resistance, apoptosis, and immune regulation (Table 3).

For the set of Exo-miR significantly modulated in LS-G6pc$^{-/-}$ mice with amyloidosis versus LS-G6pc$^{-/-}$ mice without amyloidosis, MirWalk identified 5995 targets. Pathway analysis showed significant enrichment of 51 GO biological processes and 64 KEGG pathways (adjust p-value<0.05, Supplementary Table 3). In particular, we observed an enrichment of miR-345-5p target genes involved in cancer pathways and hepatocellular carcinoma (Table 4). Of these, many genes belong to the Wnt/β-catenin signaling pathway, the apoptosis processes or are associated with transcriptional regulation by hypoxia-inducible factor 1 such as Arnt, Arnt2, Cul2, and Egln1. In addition, miR-192-5p, miR-345-5p and miR-21a-5p target genes involved in the regulation of both innate and adaptive immune responses.

As reported above, 16 Exo-miR showed modulation of expression over time. Two in particular, let-7d and miR-142-3p, displayed a significant differential positive slope between LSG6pc$^{-/-}$and WT mice. Pathway analysis carried out on let-7d and miR-142-3p showed significant enrichment of 3 GO biological processes and 38 KEGG pathways (adjust p-value<0.05, Supplementary Table 4). We again observed an enrichment of target genes involved in Wnt/β-catenin and chemokine pathway (Table 5), suggesting that these pathways may be crucial in liver disease progression. let-7d targets genes involved also in inflammatory processes or chemokine signaling pathways.

Analysis of overlapping between microRNA targets and Hallmark gene sets.

Our recent study on the proteomic analysis of LS-G6pc$^{-/-}$ and WT mouse livers (Cangelosi et al. 2019) reported evidence of metabolic reprogramming and hypoxic environment within LS-G6pc$^{-/-}$ mouse livers. On the basis of these findings, we hypothesized that exosomal microRNA may contribute to the regulation of these important biological conditions in LS-G6pc$^{-/-}$ mice. We studied the overlapping between five known Hallmark gene sets (glycolysis, hypoxia, fatty acid biosynthesis, inflammatory response and complement), retrieved from the MSigDB database version 6.2, and the targets of the microRNA significantly modulated between LS-G6pc$^{-/-}$ and WT mice. The five Hallmark gene sets were chosen based on the results obtained by proteomic analysis. Venn diagram between each Hallmark gene set and the 8384microRNA targets are shown in Figure 2. Hypergeometric tests performed on the overlapping genes reported significant overlap ($P<0.05$, Figure 2). Furthermore, analyzing the overlap between each couple of hallmark gene sets, we found that HALLMARK_HYPOXIA and HALLMARK_GLYCOLYSIS were the gene sets with the highest overlap (65 out of 200 genes, 32.5%). This indicates that genes that mostly contributed to enrichment were exclusive across gene sets, excluding that the overlap between hallmark gene sets and microRNA targets was constituted by the same set of genes.

This analysis reveals that Exo-miR significantly modulated in LS-G6pc$^{-/-}$ mice versus WT mice regulate genes connected with biological pathways previously identified by proteomic analysis as associated with reprogramming of glucose-6-phosphate and tumor development and progression.

DISCUSSION

GSD1a animal models mirroring the human pathology are indispensable for basic and translational research aimed at discovering specific targets for the development of new effective therapies. The development of HCA in LS-G6pc$^{-/-}$mice is the consequence of a single gene mutation that inhibits the G6Pase-α function and leads to liver degeneration and tumorigenesis. Thus, LS-G6pc$^{-/-}$mice are of major interest

because they mimic spontaneous HCA formation with aging and its evolution into HCC as in GSD1a patients. Thus, our animal model can be an efficient means of discovering diagnostic markers of tumor formation in livers, and mouse and human cancer may have similar molecular signatures.

In this work, we evaluated whether Exo-miR may represent potential biomarkers of GSD1a progressive pathological manifestations, liver tumor onset, and HCC development. An advantage of using the LS-G6pc$^{-/-}$mice was the possibility to perform the analysis in a homogenous model, with a common genetic background and uniform disease progression. Moreover, the mouse model utilized has allowed the clear definition of the hepatic contribution to the Exo-miR profile because the liver is the only organ affected by the deletion of the G6Pase-α in these mice. This initial approach allowed us to identify and select a restricted number of Exo-miR whose expression is modulated in LS-G6pc$^{-/-}$ mice.

Deregulation of distinct microRNA in GSD1a patients with HCA was reported for the first time by Chiu and coworkers (Chiu et al. 2014). These authors proposed mir-130b as a novel circulating biomarker for detection of GSD1a HCA. No overlapping between the results obtained by Chiu and coworkers and our results was found except for miR-21 that we found upregulated in mice with amyloidosis and not in mice with HCA. The reason for the different results obtained in the two studies is probably due to the different experimental approaches. While Chiu et al. conducted their study on liver or serum samples from GSD1a patients and healthy donors and compared the expression of selected microRNA of GSD1a HCA samples with that of HCC cell lines, we analyzed miR expression in circulating exosomes of mice and compared animals of similar age for each condition. In this respect, tissue may be more heterogeneous and possibly more prone to variations in expression of biological markers than exosomes, and mice may be more homogeneous than patients in the pathological manifestations during the progression of the disease. Moreover, some studies have shown that there may be no correlation between serum microRNA and exosomal microRNA expression levels, probably because of RNase in serum, and, thus, these two different assays cannot be substituted for each other (Zhang et al. 2019c) while in other cases difference between cancer tissues and exosomal microRNA have been reported (Warnecke-Eberz et al. 2015).

The Exo-miR we found to be deregulated in GSD1a mice with tumors are potentially relevant for the disease pathophysiology, according to the bioinformatic and literature

analysis (Chen et al. 2018; Gao et al 2017; Li et al. 2018; Zhang et al. 2019a). The signatures we have derived represent the liver specific contribution to the Exo-miR profile of HCA development. We assume that the Exo-miR differentially expressed between LS-G6pc$^{-/-}$ and control mice that have been previously reported as biomarkers of HCC or have been involved in HCC development or progression can be regarded as prognostic markers of HCC development. Further analysis may allow a correlation between Exo-miR profile and bHCA, of particular prognostic relevance for the development of HCC. Among the deregulated Exo-miR, several are particularly attractive, since they have already been proposed as biomarkers for liver diseases and liver tumorigenesis (Liu et al. 2018; Tan et al. 2015;Wang et al. 2018a; Wang et al. 2018b; Zhang et al. 2018), and may allow the identification of specific "signatures" of HCA onset and disease progression, outcome, or response to therapies. It was shown that miR-29a is down regulated in HCC and that this correlates with overexpression of claudin, a protein involved in cell migration and metastasis (Mahati et al. 2017). miR-29a suppresses growth and migration of HCC by regulating CLDN (Mahati et al. 2017)and the oncogene IGF1R(Wang et al. 2017).miR-145-5p is involved in HCC-associated signaling pathways, such as Wnt, TGF-β,and Ras, interacts with circular RNA in HCC (Qiu et al. 2019) and is one of the integrated-signature of 13 microRNA identified in HCC (Shi et al. 2015). miR-342-3p, like miR-29a,inhibits IGF-1R (Liu et al. 2018) and may serve as a biomarker for poor prognosis in HCC (Gao et al. 2017). miR-744 was identified as an independent predictor of poor prognosis in HCC (Tan et al. 2015). miR-15b-5p inhibits OIP5, an oncogenic protein regulating cell cycle progression, that was found to be upregulated in HCC (Li et al. 2017) and is considered a biomarker for diagnosis of HCC (Chen et al. 2015). Finally, miR-142-3p is a tumor suppressor that inhibits HCC cell invasion and migration(Fu et al. 2018; Tsang et al. 2015) and may therefore represent another diagnostic biomarker for HCC patients.

Four of the seven down-regulated Exo-miR (i.e., let-7i-5p, miR-29-3p, miR-342-5p and miR-744-5p) are reported as direct or indirect modulators of the expression of multiple genes and/or signaling pathways (Insulin_signaling_pathway and AMPK_signaling_pathway) relevant in glucose and lipid metabolism, suggesting their involvement in the regulation of energy metabolism reprogramming and the hypoxic condition that characterizes LS-*G6pc*$^{-/-}$ liver versus WT (Figure 3). In particular, miR-342-5p and miR-744-5p may up-regulate hepatic glucose and glycogen levels by i) controlling, directly or via AMPK, glycolytic enzymes including glucokinase (GCK),

phosphofructokinase (PFK), and pyruvate kinase (PKL) (Liu et al. 2018; Zhang et al. 2019b), ii) regulating gluconeogenesis through FOXO3 signaling pathway (Liang et al. 2013), and iii) controlling glycogen synthesis, due to their action on glycogen synthase 1 (GSK1). miR-342-5p, as well as miR-29a, may be involved, via AMPK and/or SREBP, in the up-regulation of cholesterol synthesis, through HMG-CoA reductase (HMGCR) inactivation by phosphorylation or gene induction, respectively, and in *de novo* lipogenesis, via acetil-CoA carboxylase (ACC) and fatty acid synthase (FAS) inactivation by AMPK and over-expression by SREBP, resulting in increased amount of fatty acids and triglycerides (Cheng et al. 2018; Li et al. 2013). In addition, the activity of ACC, FAS and HMGCR can be altered by miR-744-5p expression levels via AMPK signaling pathway. Finally, let-7i-5p may also contribute to the metabolism reprogramming by acting directly on lactate dehydrogenase (LDHA) gene expression, resulting in the over-production of lactate (Zhang et al. 2019b; Zhu et al. 2011). Lactate levels may be modified by miR-342-3p and let-7i-5p due to their action on HIF1α expression (Zhang et al. 2017).

Chronic inflammatory conditions may be associated with systemic amyloidosis, a serious rare pathologic complication. Amyloidosis is due to increased production of serum amyloid A protein, SAA, a non-specific acute phase protein synthesized in the liver under the control of proinflammatory cytokines. Increased SAA production may be induced by tissue damage, infection, or abnormal proinflammatory cytokine activity. SAA is deposited on several organs as insoluble amyloid fibrils that can damage tissue functions even though it may take years of chronic inflammation before manifesting itself (Simons et al. 2013). We have observed marked amyloid deposition both in vessel walls and within sinusoids in the liver (Resaz et al. 2014) and in the kidney (unpublished information) in 90% of LS-G6pc$^{-/-}$mice older than 10 months of age. These observations were confirmed by proteomic analysis that revealed that Serum Amyloid P-Component, APCS, SAA1and SAA2 were upregulated in the affected mouse livers (Cangelosi et al. 2019). The increased frequency of deposition of amyloid in LS-G6pc$^{-/-}$mice in comparison with humans affected by GSD1a may be due to the characteristic of these animals or, in general, to the difference in life span of humans vs mice. In the present study, we found that several Exo-miR were modulated in LS-G6pc$^{-/-}$mice affected by amyloidosis in comparison withLS-G6pc$^{-/-}$mice without amyloidosis. Among them, miR-192-5p andmiR-409-3pwere up regulated also in LS-G6pc$^{-/-}$ mice compared with WT, and miR-486a-5p was down regulated also in LS-

G6pc$^{-/-}$ mice compared with WT (Table 1). Moreover, miR-192-5p,miR-345-5p, miR-409-3p,miR-21a-5pand miR-150-5p have been associated with inflammatory status, and, among them, miR-345-5p, miR-21a-5p, and miR-150-5p are unique to the amyloidosis condition of the animals. Interestingly, miR-192-5p, miR-345-5p and miR-21a-5p can target genes involved in the regulation of both innate and adaptive immune responses. miR-192-5p, miR-345-5p, miR-409-3p and miR-21a-5p miR-150-5p have been associated with inflammatory status. Another Exo-miR, let-7d, targets genes involved in inflammatory processes or chemokine signaling pathways. This microRNA is downregulated in LS-G6pc$^{-/-}$ in comparison with WT mice.

The results indicate that LS-G6pc$^{-/-}$ mice have an Exo-miR signature indicating both a reduction of the mechanisms participating in the resolution of inflammation (IL-4, IL-13, IL-33), and increased activation of the pathways promoting inflammation (Bottazzi et al. 2018). The latter include IL-1a, IL-1b, lif, the IL-6 receptor (IL6ra), as well as different chemokine or chemokine receptors. Interestingly, IL-6 (Bergmann et al. 2017)and IL-1 (Sakurai et al. 2008) have been shown to contribute to the development of HCA and HCC. LS-G6pc$^{-/-}$ mice also present microRNA regulating genes involved in myeloid or lymphoid differentiation (Csf2rb, IL-3, IL-7), the latter including T, B and Innate lymphoid cells (ILCs) (Annunziato et al. 2015). These microRNA also target genes coding for molecules involved in the recruitment of immune cells in peripheral tissues and for IL-13 and IL-5, cytokines known to promote type 2 immune responses and development of chronic inflammation (Annunziato et al. 2015). In this context, a type 2-polarized microenvironment has been detected in most tumors including HCC.

References

Annunziato, F., Romagnani, C., and Romagnani, S.(2015). The 3 major types of innate and adaptive cell-mediated effector immunity. *J.Allergy Clin.Immunol.* **135**, 626-635.

Aryee, M.J., Gutierrez-Pabello, J.A., Kramnik, I., Maiti, T., and Quackenbush, J.(2009). An improved empirical bayes approach to estimating differential gene expression in microarray time-course data: BETR (Bayesian Estimation of Temporal Regulation). *BMC.Bioinformatics.* **10**, 409.

Bergmann, J., Muller, M., Baumann, N., Reichert, M., Heneweer, C., Bolik, J., Lucke, K., Gruber, S., Carambia, A., Boretius, S., Leuschner, I., Becker, T., Rabe, B., Herkel, J., Wunderlich, F.T., Mittrucker, H.W., Rose-John, S., and Schmidt-Arras, D.(2017). IL-6 trans-signaling is essential for the development of hepatocellular carcinoma in mice. *Hepatology*. **65**, 89-103.

Bottazzi, B., Riboli, E., and Mantovani, A.(2018). Aging, inflammation and cancer. *Semin.Immunol.* **40**, 74-82.

Calderaro, J., Labrune, P., Morcrette, G., Rebouissou, S., Franco, D., Prevot, S., Quaglia, A., Bedossa, P., Libbrecht, L., Terracciano, L., Smit, G.P., Bioulac-Sage, P., and Zucman-Rossi, J.(2013). Molecular characterization of hepatocellular adenomas developed in patients with glycogen storage disease type I. *J.Hepatol.* **58**, 350-357.

Cangelosi, D., Resaz, R., Petretto, A., Segalerba, D., Ognibene, M., Raggi, F., Mastracci, L., Grillo, F., Bosco, M.C., Varesio, L., Sica, A., Colombo, I., and Eva, A.(2019). A Proteomic Analysis of GSD-1a in Mouse Livers: Evidence for Metabolic Reprogramming, Inflammation, and Macrophage Polarization. *J.Proteome.Res.* **18**, 2965-2978.

Chen, Y., Chen, J., Liu, Y., Li, S., and Huang, P.(2015). Plasma miR-15b-5p, miR-338-5p, and miR-764 as Biomarkers for Hepatocellular Carcinoma. *Med.Sci.Monit.* **21**, 1864-1871.

Chen, Y., Zhang, F., Zhao, Y., He, K., Zheng, X., Pan, Y., Shao, D., Shang, P., Yang, Y., Zhang, D., Xie, Y., Yao, X., Chen, L., Li, J., and Zhang, X.(2018). Obesity-associated miR-27a upregulation promotes hepatocellular carcinoma metastasis through suppressing SFRP1. *Onco.Targets.Ther.* **11**, 3281-3292.

Chen, Y.T., Cornblath, M., and Sidbury, J.B.(1984). Cornstarch therapy in type I glycogen-storage disease. *N.Engl.J.Med.* **310**, 171-175.

Cheng, X., Li, J., and Guo, D.(2018). SCAP/SREBPs are Central Players in Lipid Metabolism and Novel Metabolic Targets in Cancer Therapy. *Curr.Top.Med.Chem.* **18**, 484-493.

Chiu, L.Y., Kishnani, P.S., Chuang, T.P., Tang, C.Y., Liu, C.Y., Bali, D., Koeberl, D., Austin, S., Boyette, K., Weinstein, D.A., Murphy, E., Yao, A., Chen, Y.T., and Li, L.H.(2014). Identification of differentially expressed microRNAs in human

hepatocellular adenoma associated with type I glycogen storage disease: a potential utility as biomarkers. *J Gastroenterol.* **49**, 1274-1284.

Chou, J.Y., Matern, D., Mansfield, B.C., and Chen, Y.T.(2002). Type I glycogen storage diseases: disorders of the glucose-6-phosphatase complex. *Curr.Mol.Med.* **2**, 121-143.

Dick, J., Kumar, N., Horsfield, C., and Jayawardene, S.(2012). AA Amyloidosis in a patient with glycogen storage disorder and progressive chronic kidney disease. *Clin.Kidney J.* **5**, 559-561.

Fu, Y., Sun, L.Q., Huang, Y., Quan, J., Hu, X., Tang, D., Kang, R., Li, N., and Fan, X.G.(2018). miR-142-3p Inhibits the Metastasis of Hepatocellular Carcinoma Cells by Regulating HMGB1 Gene Expression. *Curr.Mol.Med.* **18**, 135-141.

Gao, Y., Zhang, S.G., Wang, Z.H., and Liao, J.C.(2017). Down-regulation of miR-342-3p in hepatocellular carcinoma tissues and its prognostic significance. *Eur.Rev.Med.Pharmacol.Sci.* **21**, 2098-2102.

Hu, G., Drescher, K.M., and Chen, X.M.(2012). Exosomal miRNAs: Biological Properties and Therapeutic Potential. *Front Genet.* **3**, 56.

Labrune, P., Trioche, P., Duvaltier, I., Chevalier, P., and Odievre, M.(1997). Hepatocellular adenomas in glycogen storage disease type I and III: a series of 43 patients and review of the literature. *J.Pediatr.Gastroenterol.Nutr.* **24**, 276-279.

Li, H., Zhang, J., Lee, M.J., Yu, G.R., Han, X., and Kim, D.G.(2017). OIP5, a target of miR-15b-5p, regulates hepatocellular carcinoma growth and metastasis through the AKT/mTORC1 and beta-catenin signaling pathways. *Oncotarget.* **8**, 18129-18144.

Li, W., Yu, Z.X., and Ma, B.F.(2018). The increase of miR-27a affects the role of cisplatin on proliferation and migration capacities of liver cancer cells. *Eur.Rev.Med.Pharmacol.Sci.* **22**, 5490-5498.

Li, X., Chen, Y.T., Josson, S., Mukhopadhyay, N.K., Kim, J., Freeman, M.R., and Huang, W.C.(2013). MicroRNA-185 and 342 inhibit tumorigenicity and induce apoptosis through blockade of the SREBP metabolic pathway in prostate cancer cells. *PLoS.One.* **8**, e70987.

Liang, J., Liu, C., Qiao, A., Cui, Y., Zhang, H., Cui, A., Zhang, S., Yang, Y., Xiao, X., Chen, Y., Fang, F., and Chang, Y.(2013). MicroRNA-29a-c decrease fasting blood glucose levels by negatively regulating hepatic gluconeogenesis. *J.Hepatol.* **58**, 535-542.

Liberzon, A., Birger, C., Thorvaldsdottir, H., Ghandi, M., Mesirov, J.P., and Tamayo, P.(2015). The Molecular Signatures Database (MSigDB) hallmark gene set collection. *Cell Syst.* **1**, 417-425.

Liu, W., Kang, L., Han, J., Wang, Y., Shen, C., Yan, Z., Tai, Y., and Zhao, C.(2018). miR-342-3p suppresses hepatocellular carcinoma proliferation through inhibition of IGF-1R-mediated Warburg effect. *Onco.Targets.Ther.* **11**, 1643-1653.

Mahati, S., Xiao, L., Yang, Y., Mao, R., and Bao, Y.(2017). miR-29a suppresses growth and migration of hepatocellular carcinoma by regulating CLDN1. *Biochem.Biophys.Res.Commun.* **486**, 732-737.

Mestdagh, P., Van Vlierberghe, P., De Weer, A., Muth, D., Westermann, F., Speleman, F., and Vandesompele, J.(2009). A novel and universal method for microRNA RT-qPCR data normalization. *Genome Biol.* **10**, R64.

Qiu, L., Wang, T., Ge, Q., Xu, H., Wu, Y., Tang, Q., and Chen, K.(2019). Circular RNA Signature in Hepatocellular Carcinoma. *J.Cancer*. **10**, 3361-3372.

R Core Team. R: A language and environment for statistical computing. 2014.
Ref Type: Online Source

Resaz, R., Vanni, C., Segalerba, D., Sementa, A.R., Mastracci, L., Grillo, F., Murgia, D., Bosco, M.C., Chou, J.Y., Barbieri, O., Varesio, L., and Eva, A.(2014). Development of hepatocellular adenomas and carcinomas in mice with liver-specific G6Pase-alpha deficiency. *Dis.Model.Mech.* **7**, 1083-1091.

Sakurai, T., He, G., Matsuzawa, A., Yu, G.Y., Maeda, S., Hardiman, G., and Karin, M.(2008). Hepatocyte necrosis induced by oxidative stress and IL-1 alpha release mediate carcinogen-induced compensatory proliferation and liver tumorigenesis. *Cancer Cell*. **14**, 156-165.

Shi, K.Q., Lin, Z., Chen, X.J., Song, M., Wang, Y.Q., Cai, Y.J., Yang, N.B., Zheng, M.H., Dong, J.Z., Zhang, L., and Chen, Y.P.(2015). Hepatocellular carcinoma associated microRNA expression signature: integrated bioinformatics analysis, experimental validation and clinical significance. *Oncotarget.* **6**, 25093-25108.

Simons, J.P., Al-Shawi, R., Ellmerich, S., Speck, I., Aslam, S., Hutchinson, W.L., Mangione, P.P., Disterer, P., Gilbertson, J.A., Hunt, T., Millar, D.J., Minogue, S., Bodin, K., Pepys, M.B., and Hawkins, P.N.(2013). Pathogenetic mechanisms of amyloid A amyloidosis. *Proc.Natl.Acad.Sci.U.S.A.* **110**, 16115-16120.

Sticht, C., De La Torre, C., Parveen, A., and Gretz, N.(2018). miRWalk: An online resource for prediction of microRNA binding sites. *PLoS.One.* **13**, e0206239.

Tan, Y.L., Bai, Z.G., Zou, W.L., Ma, X.M., Wang, T.T., Guo, W., Liu, J., Li, J.S., Jie, Y., Zang, Y.J., and Zhang, Z.T.(2015). miR-744 is a potential prognostic marker in patients with hepatocellular carcinoma. *Clin.Res.Hepatol.Gastroenterol.* **39**, 359-365.

Tsang, F.H., Au, S.L., Wei, L., Fan, D.N., Lee, J.M., Wong, C.C., Ng, I.O., and Wong, C.M.(2015). MicroRNA-142-3p and microRNA-142-5p are downregulated in hepatocellular carcinoma and exhibit synergistic effects on cell motility. *Front Med.* **9**, 331-343.

Wang, F., Li, L., Piontek, K., Sakaguchi, M., and Selaru, F.M.(2018a). Exosome miR-335 as a novel therapeutic strategy in hepatocellular carcinoma. *Hepatology*. **67**, 940-954.

Wang, W., Xiao, X., Chen, X., Huo, Y., Xi, W.J., Lin, Z.F., Zhang, D., Li, Y.F., Yang, F., Wen, W.H., Yang, A.G., and Wang, T.(2018b). Tumor-suppressive miR-145 co-repressed by TCF4-beta-catenin and PRC2 complexes forms double-negative regulation loops with its negative regulators in colorectal cancer. *Int.J.Cancer*. **142**, 308-321.

Wang, X., Liu, S., Cao, L., Zhang, T., Yue, D., Wang, L., Ping, Y., He, Q., Zhang, C., Wang, M., Chen, X., Gao, Q., Wang, D., Zhang, Z., Wang, F., Yang, L., Li, J., Huang, L., Zhang, B., and Zhang, Y.(2017). miR-29a-3p suppresses cell proliferation and migration by downregulating IGF1R in hepatocellular carcinoma. *Oncotarget.* **8**, 86592-86603.

Warnecke-Eberz, U., Chon, S.H., Holscher, A.H., Drebber, U., and Bollschweiler, E.(2015). Exosomal onco-miRs from serum of patients with adenocarcinoma of the esophagus: comparison of miRNA profiles of exosomes and matching tumor. *Tumour.Biol.* **36**, 4643-4653.

Zanardi, N., Morini, M., Tangaro, M., Zamboni, F., Bosco, M.C., Varesio, L., Eva, A., Cangelosi, D.(2019). PIPE-T: a new tool for the analysis of RT-qPCR expression data. *Scientific reports*, **26**, 17550.

Zhang, C.S., Lin, Y., Sun, F.B., Gao, J., Han, B., and Li, S.J.(2019a). miR-409 down-regulates Jak-Stat pathway to inhibit progression of liver cancer. *Eur.Rev.Med.Pharmacol.Sci.* **23**, 146-154.

Zhang, J., Ma, J., Long, K., Qiu, W., Wang, Y., Hu, Z., Liu, C., Luo, Y., Jiang, A., Jin, L., Tang, Q., Wang, X., Li, X., and Li, M.(2017). Overexpression of Exosomal Cardioprotective miRNAs Mitigates Hypoxia-Induced H9c2 Cells Apoptosis. *Int.J.Mol.Sci.* **18**, 711.

Zhang, M., Li, H., Zhang, Y., and Li, H.(2019b). Oncogenic miR-744 promotes prostate cancer growth through direct targeting of LKB1. *Oncol.Lett.* **17**, 2257-2265.

Zhang, Y., Yang, L., Wang, S., Liu, Z., and Xiu, M.(2018). MiR-29a suppresses cell proliferation by targeting SIRT1 in hepatocellular carcinoma. *Cancer Biomark.* **22**, 151-159.

Zhang, Z.Y., Li, Y.C., Geng, C.Y., Wang, H.J., and Chen, W.M.(2019c). Potential Relationship between Clinical Significance and Serum Exosomal miRNAs in Patients with Multiple Myeloma. *Biomed.Res Int.* **2019**, 1575468.

Zhu, H., Shyh-Chang, N., Segre, A.V., Shinoda, G., Shah, S.P., Einhorn, W.S., Takeuchi, A., Engreitz, J.M., Hagan, J.P., Kharas, M.G., Urbach, A., Thornton, J.E., Triboulet, R., Gregory, R.I., Altshuler, D., and Daley, G.Q.(2011). The Lin28/let-7 axis regulates glucose metabolism. *Cell*. **147**, 81-94.

TABLES

Table 1 -Differentially expressed Exo-miR comparing mice with different characteristics

microRNA[a]	LS-*G6pc* $^{-/-}$ vs WT[b] (1-18 months)	HCA vs no HCA[c] (10-18 months)	Amyloid vs no Amyloid[d]. (10-18 months)
mmu-let-7i-5p	-1.67		
mmu-miR-145a-5p	-1.87	-1.97	
mmu-miR-150-5p			-1.27
mmu-miR-15b-5p	-1.86		
mmu-miR-192-5p		0.68	0.77
mmu-miR-21a-5p			0.71
mmu-miR-29a-3p	-2.40		
mmu-miR-342-3p	-1.77		
mmu-miR-345-5p			1.43
mmu-miR-409-3p	1.03		1.12
mmu-miR-486a-5p	-1.63		-1.99
mmu-miR-744-5p	-1.94		

[a] MicroRNA identifier sorted by alphabetic order. Data were analyzed by PIPE-T tool (Zanardi et al. 2019). microRNA with p value < 0.05 and log2 fold change > 0.58 or log2 fold change < -0.58 are considered significant.

[b] Log2 fold change comparing the expression of microRNA between 45 LS-*G6pc* $^{-/-}$ and 18 WT mice. Positive values indicate upregulation **in LS-*G6pc* $^{-/-}$ mice**. Analysis was carried out using animals with comparable ages ranging from 1 to 18 months as **indicated** between brackets.

[c] Log2 fold change comparing the expression of microRNA between 16 LS-*G6pc* $^{-/-}$ mice with HCA and 14 LS-*G6pc* $^{-/-}$ mice without HCA. Positive values indicate upregulation in LS-*G6pc* $^{-/-}$ mice with HCA. Analysis was carried out using animals with comparable ages ranging from 10 to 18 months as indicated between brackets. The 16 mice analyzed developed multiple tumors, for a total of 53 lesions: 15 IHCA, 14 UHCA, 16 bHCA, 5 early HCC and 3 HCC.

[d] Log2 fold change comparing the expression of microRNA between 13 LS-*G6pc* $^{-/-}$ mice with amyloidosis and 17 LS-*G6pc* $^{-/-}$ mice without amyloidosis. Positive values indicate upregulation in LS-*G6pc* $^{-/-}$ mice with amyloidosis. Analysis was carried out using animals with comparable ages ranging from 10 to 18 months as indicated between brackets.

Table 2. Target genes of Exo-miR significantly modulated in LS-G6pc$^{-/-}$ mice.

MicroRNA	Pathway	miR-744-5p	miR-342-3p	let-7i-5p
Bax	Apoptosis	+		
Bcl2l11		+		
Casp7				+
Ccl22	Chemokine	+		
Ccl5		+		
Ccl6		+		
Ccl9		+		
Cxcl1		+		
Cxcl10		+		
Cxcl12		+		
Cxcl13		+		
Ccr2		+		
Ccr9		+		
Cx3cr1		+		
Cxcr2		+		
Cxcr5		+		
Il12a	Cytokine			+
Il13				+
Il5				+
Il7				+
Csf2rb				+
Csf2rb2				+
Il13ra1				+
Il6ra				+
Il7r				+
G6pc	GSD1a	+		
Phkg2	GSD IX	+		
Gck	Glucose metabolism	+		
Pfkfb3				+
Pfkl				+
Pklr		+		
Gys1	Glycogen metabolism	+	+	
Gsk3b		+	+	

Igf1	Insulin	+		
Insr			+	
Irs3		+		
Irs4			+	
Prkaa1		+	+	
Prkaa2		+		
Prkab2		+		
Prkag3		+		
Pklr		+		
G6pc		+		
Ppp1r3a	Diabetes	+		
Ptpn1		+		
Prkab2	Fatty acid and cholesterol	+		
Prkag3		+		
Slc2a2		+		
Foxo3	AMPK	+		
G6pc		+		
Hmgcr		+		
Pfkbp2		+		
Pfkbp3		+		
Pfkbp4		+		
Pfkl		+		
Ppargc1a		+		
Prkaa1		+		
Prkaa2		+		
Prkab2		+		
Prkag3		+		
Apc2	Wnt			+
Appl1				+
Frat1			+	
Frat2			+	
Fzd2			+	+
Fzd5				+
Fzd8				+
Lrp6				+
Stk4		+		+
Tcf7l1			+	
Wnt8b				+
Zbtb16			+	

miR-744-5p, miR-342-3p, and let-7i-5p target genes, specifically involved in the indicated pathways, are shown.

Table 3. Target genes of Exo-miR significantly modulated in LS-G6pc$^{-/-}$ mice with HCA

Gene target	Pathway	miR-192-5p
Agap2	FOXO1	+
Atm		+
Nras		+
Pik3ca		+
Pik3r1		+
Prkab2		+
Prkag3		+
Atm	Regulation of Telomere Maintenance	+
Ercc4		+
Hnrnpu		+
Map2k7		+
Nek2		+
Ppp1r10		+
Braf	Hepatocellular Carcinoma	+
E2f2		+
Frat1		+
Igf2		+
Nras		+
Pik3ca		+
Pik3r1		+
Prkcb		+
Tcf7		+

miR-192-5p target genes, specifically involved in the indicated pathways, are shown.

Table 4. Target genes of Exo-miR significantly modulated in LS-G6pc$^{-/-}$ mice with amyloidosis

Pathway	Target Gene	miR-345-5p	miR-21a-5p	miR-150-5p	miR-192-5p
Apoptosis	Bax	+			
	Bcl2	+			
	Bcl2l11	+			
	Bid	+			
	Birc5	+			
Hypoxia	Arnt	+			
	Arnt2	+			
	Cul2	+			
	Egln1	+			
Cytokine	Il13				+
	Il3ra				+
	Il4ra				+
	Il6st				+
	Stat6	+			+
	Il33		+		
Innate immunity	Tlr4	+	+		
Adaptive immunity	Nfatc1, 2, 4			+	
Insulin	Ywhaz	+			
TGFb	Smad2	+			
Wnt	Apc2	+			
	Frat1	+			
	Fzd1	+			
	Fzd3	+			
	Fzd9	+			
	Wnt1	+			
	Wnt2	+			
	Wnt2b	+			
	Wnt5a	+			
	Wnt9a	+		+	

miR-345-5p, miR-21a-5p, miR-150-5p, and miR-192-5p target genes, specifically involved in the indicated pathways, are shown.

Table 5. Target genes of Exo-miR significantly modulated in LS-G6pc$^{-/-}$ mice over time

Pathway	Genes	let-7d	miR-142-3p
Anaerobic glycolysis	Ldha	+	
Cholesterol	Lamtor1	+	
Glucose metabolism	Hk2	+	
	Pdk1	+	
	Pfkfb3	+	
	Pfkl	+	
Innate immunity	Lyn	+	
	Tlr4	+	
Cytokine	Il1a	+	
	Il1b	+	
	Lif	+	
	Lifr	+	
	Il6ra	+	
Chemokine	Ccl22	+	
	Ccl3	+	
	Ccl9	+	
	Cxcl9	+	
	Ccr9	+	
	Ccr10	+	
	Ccr1	+	
Wnt	Apc2	+	
	Ctnnb1	+	
	Csnk1a1	+	
	Csnk1g1	+	
	Dkk1	+	
	Dvl1	+	
	Fbxw11	+	
	Fzd1	+	
	Fzd3	+	
	Lrp5	+	
	Lef1	+	
	Nkd1	+	
	Nlk	+	
	Psen1	+	
	Sfrp5	+	
	Tcf7	+	
	Tcf7l1	+	
	Vangl1	+	
	Wnt3	+	
	Wnt9a	+	

Positive regulation of small GTPase mediated signal transduction and MAPK	Abra		+
	Arpp19		+
	Arrb1		+
	Bdnf		+
	Cacna1a		+
	Cacna1c		+
	Cacna1i		+
	Cdc42		+
	Cdon		+
	Dusp3		+
	Fgf16		+
	Gm5127		+
	Gpr174		+
	Igf1		+
	Map2k2		+
	Mapk1		+
	Mapk8		+
	Mapk9		+
	Nrg1		+
	Ntrk2		+
	Ppm1b		+
	Rasgrp1		+
	Rras2		+
	Rtn4		+
	Stk4		+
	Taok1		+
	Traf2		+

Let-7d and miR-142-3p target genes, specifically involved in the indicated pathways, are shown.

Figures

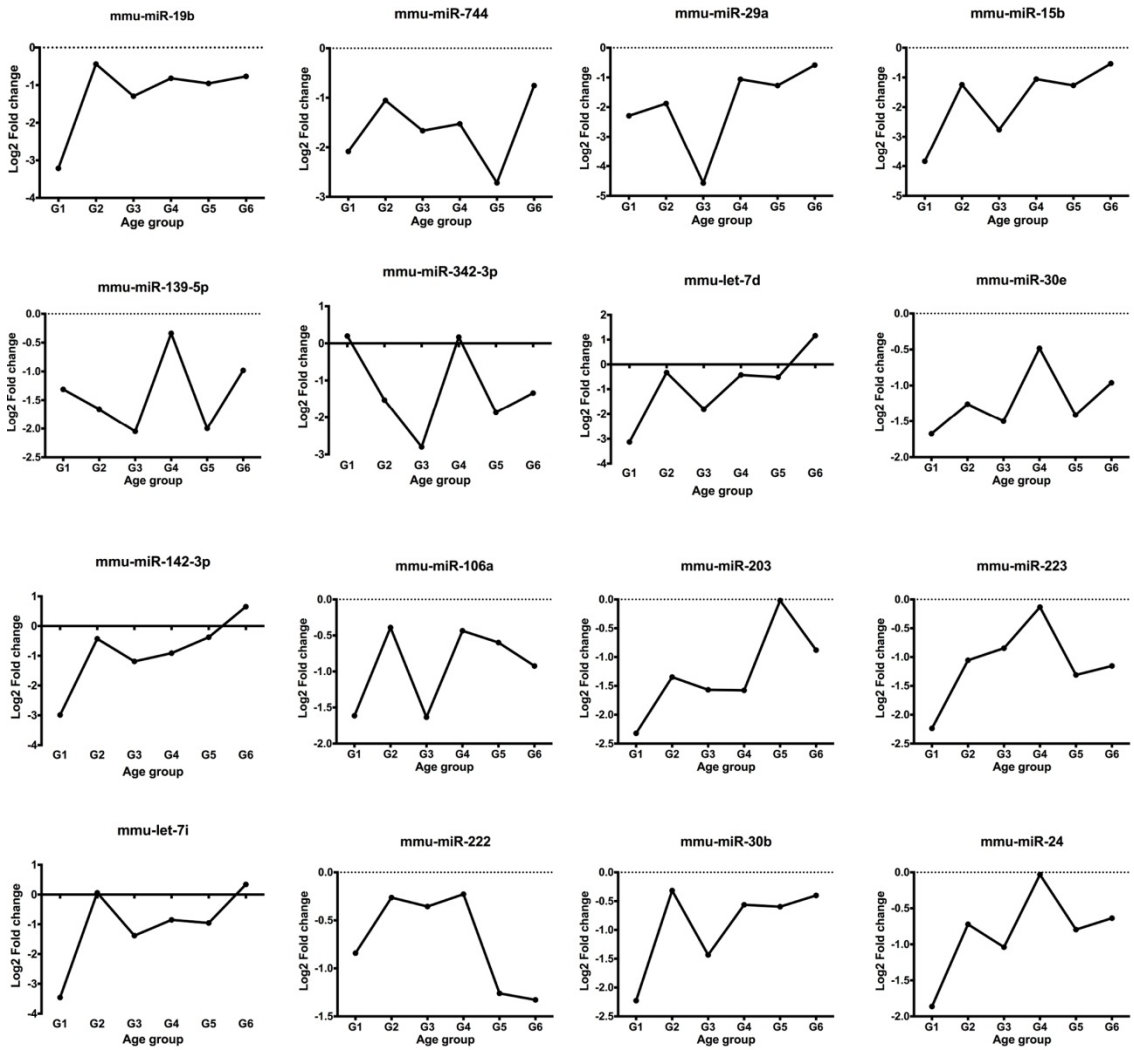

Figure 1 - Time course analysis reveals an age dependent modulation of microRNA expression

The plots show the median log2 fold change value for the 16 significant differentially represented Exo-miR identified by BETR method between LS-G6pc$^{-/-}$ and WT mice grouped by age. The name of the microRNA is reported on top of each plot.

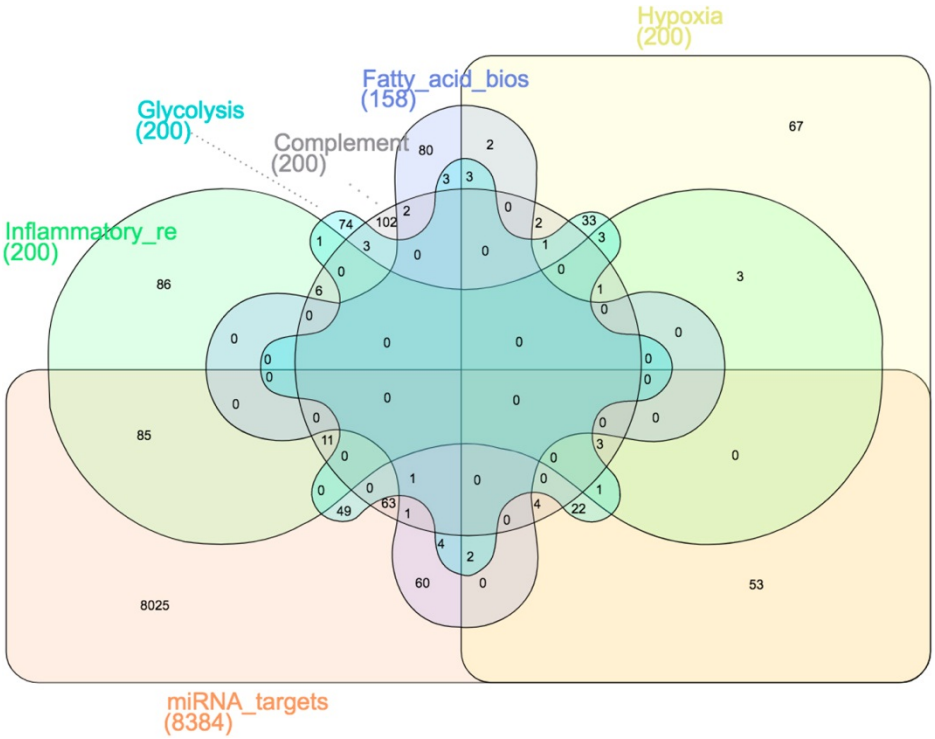

Figure 2 - Venn diagram among five selected hallmark gene sets

Venn diagram showing exclusive and common genes among all possible combinations of five GSEA hallmark gene sets and Exo-miR targets gene set. Each combination is depicted by a distinct shape and color. Grey dots link gene set name and gene set shape when the gene set name could not be inserted above the shape. The GSEA gene sets used in the analysis belong to the Hallmark collection of the Molecular Signature Database (MSigDB) v6.2 database. A simplified colored name is reported for each MSigDB gene set for readability. The full MSigDB gene set names are:

HALLMARK_HYPOXIA, HALLMARK_GLYCOLYSIS,
HALLMARK_FATTY_ACID_BIOSYNTHESIS,
HALLMARK_INFLAMMATORY_RESPONSE, and
HALLMARK_COMPLEMENT.

The number of genes of each MSigDB gene set is reported between brackets below the gene set name. The targets of the Exo-miR significantly modulated in LS-G6pc$^{-/-}$ versus WT mice analysis was organized into a gene set and referred to as miRNA targets. Exo-miR targets were identified using MirWalk tool. Venn diagram was drawn using InteractiVenn tool.

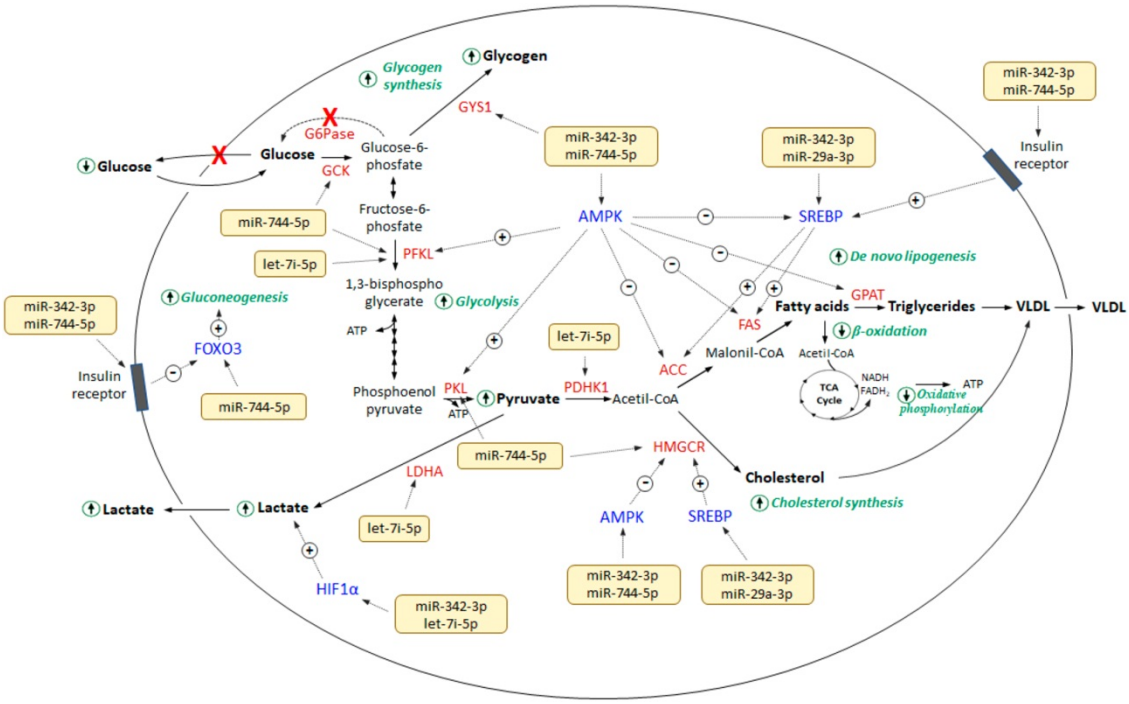

Figure 3 – Diagram showing the interaction among the deregulated miR and targets relevant in glucose and lipid metabolism.

Supplementary files

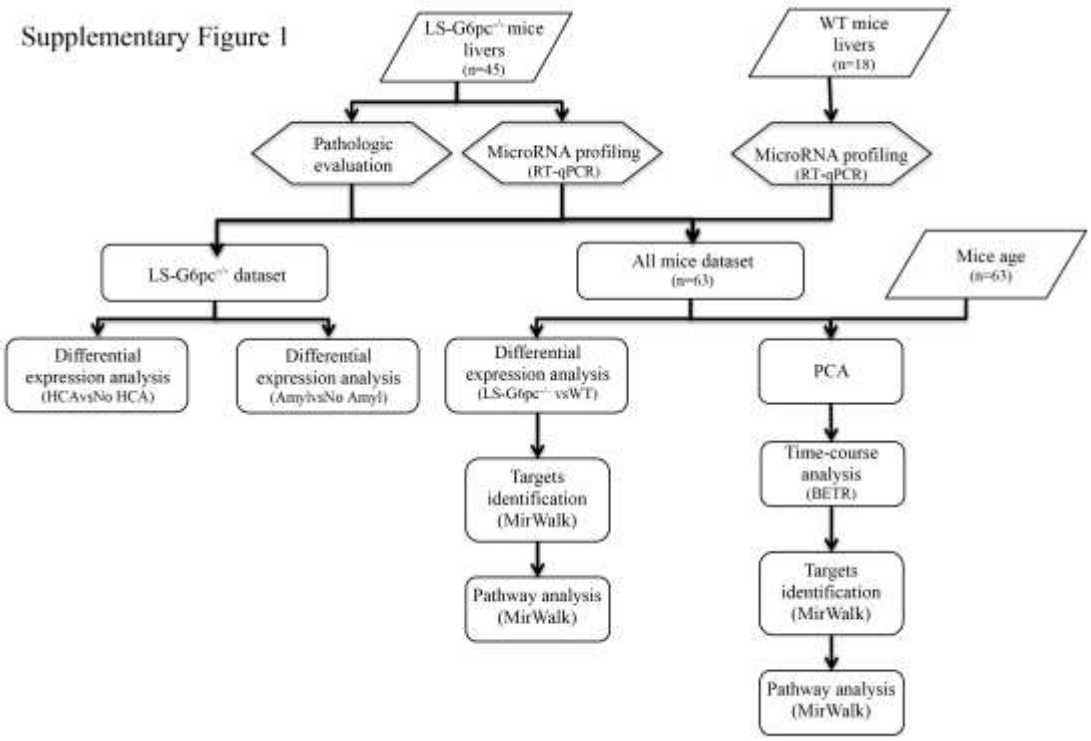

Figure S1- Schematic representation of the whole bioinformatic strategy used in the study. The microRNA representation profile of 45 LS-G6pc$^{-/-}$ and 18 WT mouse plasma exosomes was measured by ViiA 7 RT-qPCR. Pathological evaluation of the livers assessed the presence of hepatic adenomas and/or amyloidosis within the entire set of mice samples. Differential expression analysis assessed any significant modulation of the Exo-miR between groups of LS-G6pc$^{-/-}$ and WT mice, LS-G6pc$^{-/-}$ mice characterized by the presence\absence of hepatic adenomas, or LS-G6pc$^{-/-}$ mice characterized by the presence/absence of amyloidosis. The representation profile of LS-G6pc$^{-/-}$ and WT mice over 6 distinct age groups was compared using BETR method. Analysis identified age-dependent modulated Exo-miR whose targets were identified using MirWalk tool. Pathway analysis on these targets identified the most significantly altered biological processes and pathways.

Supplementary Figure 2

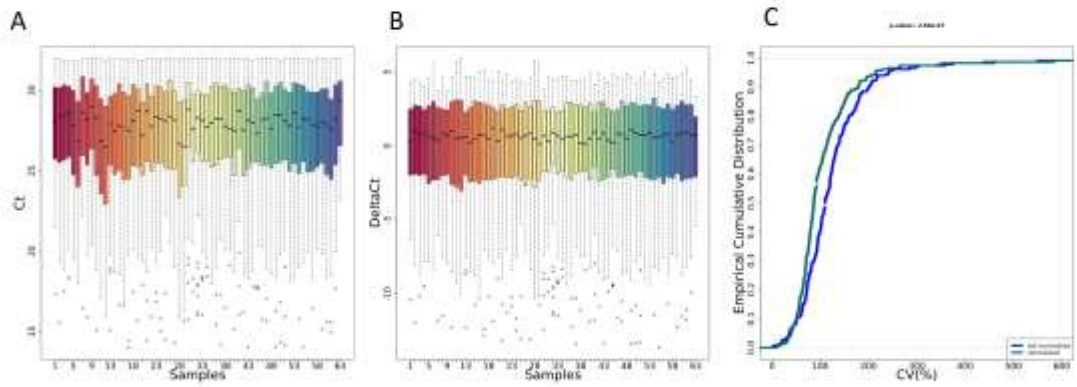

Figure S2 - Qualitative and quantitative assessment of the noise reduction for LS-G6pc$^{-/-}$ and WT mice data

The box plots reported in panels A and B show the distribution of Ct and delta Ct values for every samples before and after data normalization, respectively. The plot reported in panel C show the ECDFs (y axis) and the coefficient of variation (CV) for every samples before (blue line) and after (Green line) data normalization. Kolmogorov-Smirnov test assessed the significance of the separation between the curves and the p-value is reported on top of the plot. P-value lower than 0.05 is considered significant. Global mean was used to normalize the data.

Supplementary Figure 3

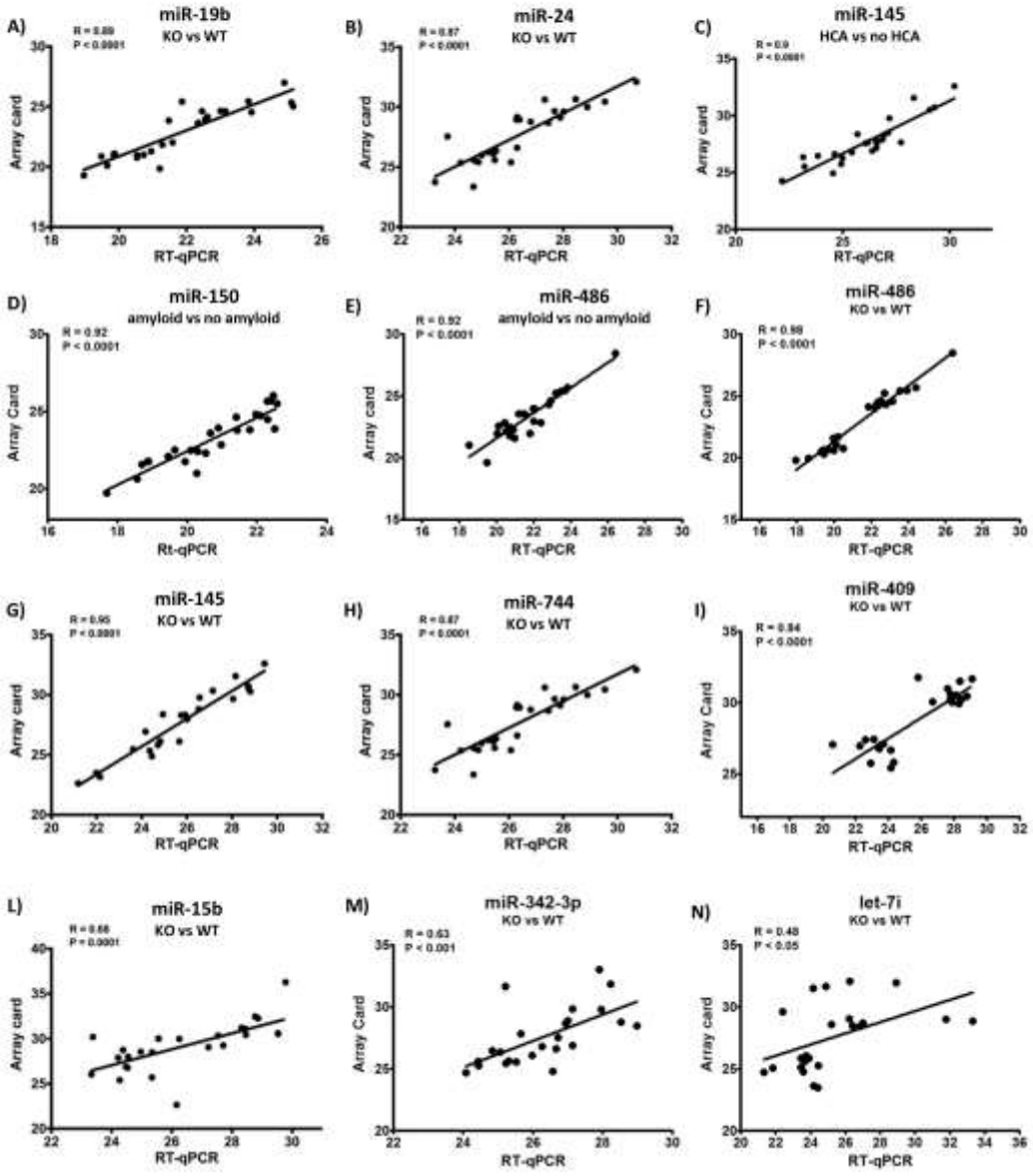

Figure S3 - Scatter plots of Ct values measured by RT-qPCR and Array card

A scatter plot showing correlation between the expression values measured by RT-qPCR and Array card on LS-G6pc$^{-/-}$ and WT mice samples is depicted for a selection of significant Exo-miR**.** Each point is the Ct value of a sample measured by RT-qPCR and Array card. Correlation is assessed by Pearson method. Linear regression line is superimposed to the points within each plot. Pearson correlation and p-value are reported in the top left side of the plots.

Supplementary Figure 4

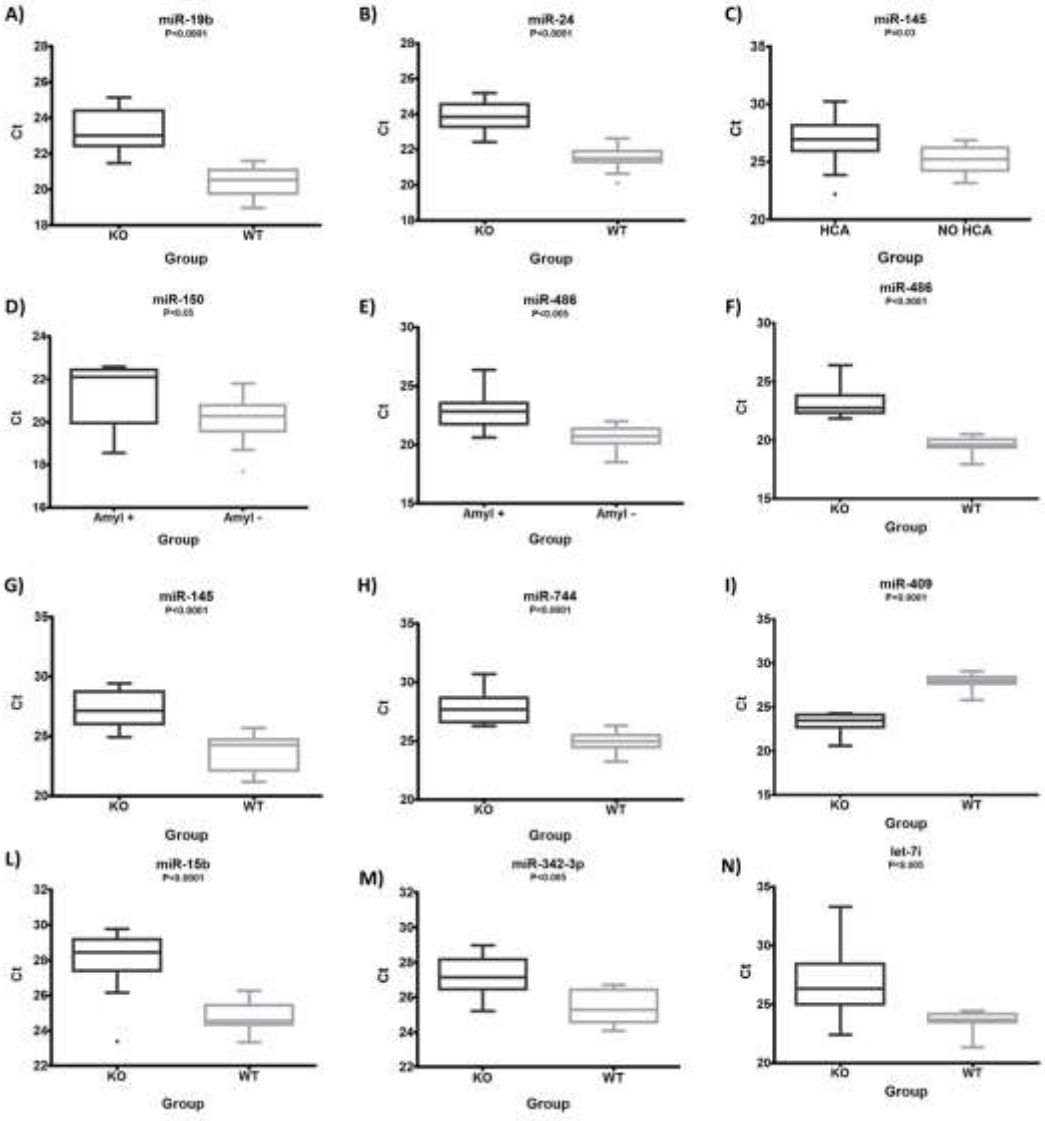

Figure S4- Box plots of Ct values measured by RTqPCR between LS-G6pc$^{-/-}$ and WT mice; LS-G6pc$^{-/-}$ mice with and without amyloidosis; LS-G6pc$^{-/-}$ mice with and without adenoma.

Box-plots showing the differential expression between LS-G6pc$^{-/-}$ and WT mice, between LS-G6pc$^{-/-}$ mice with and without amyloidosis and between LS-G6pc$^{-/-}$ mice with and without adenoma are depicted for a selection of significant Exo-miR. Ct values were measured by RTqPCR. Statistical significance of the difference is assessed by unpaired t-test. P values and the name of the microRNA are reported on the top of each plot.

Supplementary Table 1

Name	Hits	Pop Hits	List Total	Pop Total	Genes	Pvalue	adjusted Pvalue (BH)	Ontology	MicroRNA
mmu04010_MAPK_signaling_pathway	43	294	558	8275	110651;12064;12288;12296;12531;12929;13638;13712;13714;13869;14172;14180;14184;16000;16151;16180;17260;17346;17347;17762;18015;18021;18212;19059;193740;21812;21813;22030;23797;23882;26397;26401;26405;26412;26414;26416;26921;30957;320139;58231;67603;78390;80857	0	0	KEGG	mmu-let-7i-5p
mmu04910_Insulin_signaling_pathway	48	140	1369	8275	103988;105787;108079;108097;109880;11651;11652;12313;12315;12703;12928;12929;13684;13685;140491;14252;14377;14784;15461;16150;16369;17346;17347;18176;18706;18708;18709;18710;18762;18770;19017;19062;19084;19087;19088;19246;20416;216148;218268;241113;26413;26419;26420;271849;56637;68961;72508;74769	0	0	KEGG	mmu-miR-744-5p
mmu04722_Neurotrophin_signaling_pathway	43	121	1369	8275	108960;109880;11651;11652;11848;12028;12064;12070;12313;12315;12928;12929;14784;15461;16150;16923;18036;18053;18176;18212;18706;18708;18709;18710;192662;20112;20416;20661;216148;22034;22059;26413;26415;26416;26419;26420;266632;271849;327826;56484;56637;74769;77480	0	0	KEGG	mmu-miR-744-5p
mmu04917_Prolactin_signaling_pathway	29	72	1369	8275	103988;11651;11652;12443;12703;14784;15461;16362;18176;18706;18708;18709;18710;19116;20416;20526;20851;216148;22373;26413;26415;26416;26419;26420;271849;56468;56484;56637;74769	0.0001	0.007	KEGG	mmu-miR-744-5p
mmu04152_AMPK_signaling_pathway	43	126	1369	8275	105787;108079;108097;11549;11651;11652;12283;12443;13685;14377;15357;15378;15568;16000;16369;170768;18640;18641;186	0.0001	0.007	KEGG	mmu-miR-744-5p

					42;18706;18708;18709;18710;19017;19054;19325;20250;207565;231991;241113;26931;269643;270198;30049;329065;56484;57915;59032;68365;68465;72508;72674;74769				
mmu04660_T_cell_receptor_signaling_pathway	36	101	1369	8275	11651;11652;11848;12042;12487;12500;12503;12525;14784;15461;16150;16151;16191;16822;17444;17974;18018;18036;18176;18566;18706;18708;18709;18710;19059;21947;22325;26413;26415;26416;26420;53859;54167;56637;57257;74769	0.0002	0.0113	KEGG	mmu-miR-744-5p
mmu05164_Influenza_A	50	168	1369	8275	106759;11651;11652;11909;12371;142980;14961;14969;15001;15002;15463;15945;15975;16150;16159;16646;16647;18036;18550;18706;18708;18709;18710;18750;19106;20304;21898;21933;228607;232989;237082;24014;246728;26398;26413;26415;26416;26419;26420;266632;50528;53319;54196;56488;56489;56637;58185;66824;74769;81489	0.0004	0.0188	KEGG	mmu-miR-744-5p
mmu04012_ErbB_signaling_pathway	30	84	1369	8275	109880;11352;11651;11652;12576;12928;12929;13685;13874;14784;15461;17974;18176;18706;18708;18709;18710;18750;20416;20851;216148;21802;26398;26413;26419;26420;271849;56637;72508;74769	0.0005	0.0201	KEGG	mmu-miR-744-5p
mmu04062_Chemokine_signaling_pathway	56	199	1369	8275	109880;11651;11652;11848;12145;12765;12769;12772;12928;12929;13051;140580;14678;14696;14701;14708;14709;14784;14825;15461;15945;16150;16151;17969;18036;18176;18706;18708;18709;18710;18762;18796;19303;19878;20299;20304;20305;20308;20315;20416;20851;216148;216869;21844;22325;23832;24013;26413;271849;30955;320129;55985;56484;56637;57257;74769	0.0006	0.0212	KEGG	mmu-miR-744-5p
mmu01521_EGFR_tyrosine_kinase_inhibitor_resistance	28	80	1369	8275	109880;11651;11652;12028;12125;13684;13685;14784;15461;16000;18176;18591;18596;18706;18708;18709;18710;18750;20416;	0.001	0.0217	KEGG	mmu-miR-744-5p

					216148;21802;218268;26413;271849;56484;56637;72508;74769				
mmu05220_Chronic_myeloid_leukemia	27	76	1369	8275	109880;11651;11652;12028;12443;12571;12576;12928;12929;13016;14784;15461;16150;16151;17127;18176;18706;18708;18709;18710;20416;20851;216148;22059;26413;271849;74769	0.001	0.0217	KEGG	mmu-miR-744-5p
mmu05214_Glioma	26	71	1369	8275	109880;11651;11652;12028;12313;12315;12443;12571;14784;15461;16000;18176;18591;18596;18706;18708;18709;18710;18750;20416;216148;21802;22059;26413;271849;74769	0.0009	0.0217	KEGG	mmu-miR-744-5p
mmu05210_Colorectal_cancer	30	88	1369	8275	109880;11651;11652;11799;11848;12028;12125;12367;12371;12387;12443;13874;14784;15461;17126;17127;18176;18706;18708;18709;18710;21802;22059;26413;26419;26420;56637;58801;72508;74769	0.001	0.0217	KEGG	mmu-miR-744-5p
mmu04014_Ras_signaling_pathway	63	233	1369	8275	11352;11600;11651;11652;11848;12064;12313;12315;12977;13636;13638;13640;14164;14165;14182;14696;14701;14708;14709;14784;14810;15461;16000;16150;16151;17311;18053;18176;18212;18591;18596;18654;18706;18708;18709;18710;18750;18806;19344;19414;19418;19732;19765;20416;216148;21802;21844;225845;226525;237625;23871;26413;26419;26420;26971;271849;333050;58231;66350;66482;72399;74055;74769	0.0007	0.0217	KEGG	mmu-miR-744-5p
GO:0045663_positive regulation of myoblast differentiation	6	28	332	12262	12226;17260;17329;20307;57810;319594	0.0003	0.0219	GOBP	mmu-miR-29a-3p
mmu04723_Retrograde_endocannabinoid_signaling	12	150	243	8275	12288;14401;14402;14681;14688;14700;14701;14706;16522;216227;407785;53623	0.0029	0.0253	KEGG	mmu-miR-342-3p
mmu04920_Adipocytokine_signaling_pathway	8	71	243	8275	105787;16151;16370;19013;19247;207565;50790;74205	0.0021	0.0253	KEGG	mmu-miR-342-3p
mmu04150_mTOR_signaling_pathway	13	153	243	8275	105787;12283;16337;18607;18710;20662;227743;26987;329679;56637;57265;68441;7	0.0012	0.0253	KEGG	mmu-miR-342-3p

					8757				
mmu04151_PI3K-Akt_signaling_pathway	22	358	243	8275	105787;11600;13874;14175;14176;14688;14700;14701;14706;14936;16151;16337;16399;16410;170755;18595;18607;18710;20662;26987;53978;56637	0.0021	0.0253	KEGG	mmu-miR-342-3p
mmu04713_Circadian_entrainment	10	98	243	8275	11517;12288;14681;14688;14700;14701;14706;16522;234889;53623	0.0012	0.0253	KEGG	mmu-miR-342-3p
mmu04660_T_cell_receptor_signaling_pathway	10	101	243	8275	16151;18018;18021;18607;18710;19264;19419;20662;54167;56637	0.0015	0.0253	KEGG	mmu-miR-342-3p
mmu04727_GABAergic_synapse	10	88	243	8275	12288;14401;14402;14645;14681;14688;14700;14701;14706;16522	0.0006	0.0253	KEGG	mmu-miR-342-3p
mmu05226_Gastric_cancer	12	150	243	8275	12591;14175;14176;14296;17126;17127;18710;20662;212398;21415;56637;57265	0.0029	0.0253	KEGG	mmu-miR-342-3p
mmu04724_Glutamatergic_synapse	11	114	243	8275	12288;14645;14681;14688;14700;14701;14706;14806;216227;26556;53623	0.0011	0.0253	KEGG	mmu-miR-342-3p
mmu05032_Morphine_addiction	9	92	243	8275	14401;14402;14681;14688;14700;14701;14706;16522;18575	0.0027	0.0253	KEGG	mmu-miR-342-3p
mmu04014_Ras_signaling_pathway	16	233	243	8275	11600;14175;14176;14688;14700;14701;14706;16151;16337;18015;18595;18710;19247;19419;20662;23871	0.0029	0.0253	KEGG	mmu-miR-342-3p
mmu04392_Hippo_signaling_pathway	5	26	189	8275	213391;215653;27373;68473;97064	0.0006	0.0276	KEGG	mmu-miR-29a-3p
mmu04721_Synaptic_vesicle_cycle	23	62	1369	8275	108124;11772;11773;11964;11966;11974;11975;11984;12287;13430;140919;18195;20508;20907;20908;20910;22318;225644;235415;338375;66144;66290;74325	0.0015	0.0282	KEGG	mmu-miR-744-5p
mmu04150_mTOR_signaling_pathway	44	153	1369	8275	105787;108079;109270;109880;11651;11652;11848;11964;11966;12283;13684;13685;14245;14362;14365;14366;14784;15461;16000;16150;18176;18706;18708;18709;18710;18750;20112;216742;218268;22423;227743;252875;26413;329679;338375;56637;66144;66290;67046;72508;74769;75705;78757;97998	0.0015	0.0282	KEGG	mmu-miR-744-5p
mmu04930_Type_II_diabetes_	19	48	1369	8275	103988;12287;12703;16150;16369;16514;1	0.002	0.0295	KEGG	mmu-miR-

mellitus					8706;18708;18709;18710;18746;18754;18762;18770;20526;26413;26419;26420;74769				744-5p
mmu04130_SNARE_interactions_in_vesicular_transport	15	33	1369	8275	20333;20907;20908;22317;22318;22319;228960;53330;53334;53611;53620;54399;55943;58244;67727	0.0021	0.0295	KEGG	mmu-miR-744-5p
mmu05142_Chagas_disease_(American_trypanosomiasis)	32	101	1369	8275	106759;11651;11652;12062;12500;12503;14672;14678;14680;14681;16150;16151;16159;17126;17127;18706;18708;18709;18710;18796;20304;21898;22034;26398;26413;26415;26416;26419;26420;266632;269643;74769	0.0018	0.0295	KEGG	mmu-miR-744-5p
mmu04068_FoxO_signaling_pathway	39	132	1369	8275	105787;108079;108097;109880;11651;11652;12125;12443;12576;12581;14377;14784;15461;16000;16150;16369;17126;17127;18176;18706;18708;18709;18710;216439;241113;252870;26413;26415;26416;26419;26420;26556;26557;56484;58231;66822;67731;73251;74769	0.0018	0.0295	KEGG	mmu-miR-744-5p
mmu04010_MAPK_signaling_pathway	73	294	1369	8275	109880;11600;11651;11652;11909;12064;12287;12296;12297;12298;12300;12367;12928;12929;12977;13636;13638;13640;13714;13874;14164;14165;14182;14701;14784;15461;16000;16150;16151;16180;17187;17260;17311;17346;17347;17762;18018;18053;18176;18212;18591;18596;18654;18750;19043;19059;192176;19418;20112;216869;21802;22034;22059;235584;239556;26398;26404;26413;26415;26416;26419;26420;266632;319734;53859;54376;58231;66513;71751;72349;75590;76089;81904	0.0021	0.0295	KEGG	mmu-miR-744-5p
mmu04144_Endocytosis	68	270	1369	8275	100017;116733;11772;11773;11840;11842;11848;12340;12765;13196;13430;13660;13855;13858;140500;14275;15006;15007;15018;15461;16185;16396;16572;16835;17126;17127;17999;18720;18762;18806;19157;19158;19325;19344;19349;194309;20844;215	0.0022	0.0295	KEGG	mmu-miR-744-5p

mmu05160_Hepatitis_C	39	134	1369	8275	280;216439;216869;218441;22034;22187;228998;232227;24013;243621;28084;30930;320129;52348;54673;55988;56433;56440;58220;67064;68524;69091;69178;72183;72318;74325;74998;75767;75788;77038;84092106759;109880;11651;11652;12741;142980;14784;15461;15975;16150;16151;16362;16835;18176;18260;18417;18706;18708;187099;18710;19106;19192;22031;22034;22059;228607;24014;242653;246728;26413;26415;26416;26419;26420;269643;56489;56637;60363;74769	0.0023	0.0295	KEGG	mmu-miR-744-5p
mmu04910_Insulin_signaling_pathway	11	140	243	8275	105787;14936;16337;16370;18607;18710;18759;20662;26987;54646;56637	0.0048	0.0384	KEGG	mmu-miR-342-3p
mmu05200_Pathways_in_cancer	60	530	558	8275	11864;12313;12322;12369;12394;12571;12579;12828;12829;12929;12983;12984;13712;14172;14180;14184;14367;14370;14688;14702;14865;15251;16000;16151;16159;16163;16164;16191;16194;16196;16197;16452;16974;17126;17977;18796;19211;19225;19713;19878;21812;21813;22030;22423;237977;23805;23882;26414;269608;27412;432530;53978;54354;56198;57265;58231;67923;72993;74769;80857	0.0004	0.0392	KEGG	mmu-let-7i-5p
mmu04668_TNF_signaling_pathway	33	110	1369	8275	11651;11652;11909;12367;12977;14825;15945;16150;16151;16362;16396;18706;18708;18709;18710;20304;22031;231991;26398;26413;26415;26416;26419;26420;53859;66513;66724;67384;69601;72542;74006;74568;74769	0.0032	0.0392	KEGG	mmu-miR-744-5p
mmu04726_Serotonergic_synapse	10	132	243	8275	12288;14401;14402;14681;14688;14700;14701;14706;15550;16522	0.0086	0.0401	KEGG	mmu-miR-342-3p
mmu04960_Aldosterone-regulated_sodium_reabsorption	5	38	243	8275	16337;18607;18710;65962;83814	0.0077	0.0401	KEGG	mmu-miR-342-3p
mmu04926_Relaxin_signaling_pathway	10	131	243	8275	14681;14688;14700;14701;14706;17126;17127;17395;18710;20662	0.0082	0.0401	KEGG	mmu-miR-342-3p

mmu04068_FoxO_signaling_pathway	10	132	243	8275	105787;16337;16370;170755;17126;17127;18607;18710;20662;26556	0.0086	0.0401	KEGG	mmu-miR-342-3p
mmu04725_Cholinergic_synapse	9	113	243	8275	12288;14681;14688;14700;14701;14706;16522;18710;226922	0.0092	0.0401	KEGG	mmu-miR-342-3p
mmu04211_Longevity_regulating_pathway	8	90	243	8275	105787;12421;16337;16370;18710;207565;26987;77683	0.0076	0.0401	KEGG	mmu-miR-342-3p
mmu04921_Oxytocin_signaling_pathway	11	153	243	8275	105787;107589;12288;12298;14681;16522;17904;18018;18021;207565;234889	0.0086	0.0401	KEGG	mmu-miR-342-3p
mmu04390_Hippo_signaling_pathway	11	154	243	8275	104318;12162;17126;17127;17131;18759;21415;23859;50523;56637;57265	0.009	0.0401	KEGG	mmu-miR-342-3p
mmu04080_Neuroactive_ligand-receptor_interaction	17	289	243	8275	11435;11517;13610;14401;14402;14427;14739;14806;15550;18389;18438;193034;216749;22355;228139;53623;53978	0.0089	0.0401	KEGG	mmu-miR-342-3p
mmu04810_Regulation_of_actin_cytoskeleton	14	215	243	8275	107589;14175;14176;14701;16399;16410;18595;18710;18718;20662;219140;22330;53978;56378	0.0076	0.0401	KEGG	mmu-miR-342-3p
GO:0010640_regulation of platelet-derived growth factor receptor signaling pathway	5	25	332	12262	16948;19255;19271;75725;93692	0.0011	0.0402	GOBP	mmu-miR-29a-3p
GO:0034620_cellular response to unfolded protein	7	76	332	12262	13163;13666;19255;76867;77128;231630;328572	0.0067	0.0408	GOBP	mmu-miR-29a-3p
GO:0002067_glandular epithelial cell differentiation	6	57	332	12262	12571;12753;15378;19130;19726;22417	0.0066	0.0408	GOBP	mmu-miR-29a-3p
GO:1903312_negative regulation of mRNA metabolic process	7	81	332	12262	18772;22083;22695;53379;75420;230257;230908	0.0091	0.0408	GOBP	mmu-miR-29a-3p
GO:0045445_myoblast differentiation	9	93	332	12262	12226;17260;17329;18740;20307;57810;69564;102423;319594	0.0017	0.0408	GOBP	mmu-miR-29a-3p
GO:0048008_platelet-derived growth factor receptor signaling pathway	6	62	332	12262	14158;16948;19255;19271;75725;93692	0.0094	0.0408	GOBP	mmu-miR-29a-3p
GO:0019080_viral gene expression	6	57	332	12262	16865;22695;98415;230908;233532;328572	0.0066	0.0408	GOBP	mmu-miR-29a-3p
GO:0002066_columnar/cuboidal epithelial cell development	7	74	332	12262	12571;12753;15378;19726;77929;229320;319801	0.0059	0.0408	GOBP	mmu-miR-29a-3p

GO:0090109_regulation of cell-substrate junction assembly	6	57	332	12262	14260;19271;20874;22417;105352;110829	0.0066	0.0408	GOBP	mmu-miR-29a-3p
GO:1901888_regulation of cell junction assembly	8	83	332	12262	14260;16150;19271;20874;22417;83814;105352;110829	0.003	0.0408	GOBP	mmu-miR-29a-3p
GO:0033209_tumor necrosis factor-mediated signaling pathway	6	60	332	12262	15257;16150;19255;21873;84094;110829	0.0082	0.0408	GOBP	mmu-miR-29a-3p
GO:0019083_viral transcription	5	44	332	12262	22695;98415;230908;233532;328572	0.0095	0.0408	GOBP	mmu-miR-29a-3p
GO:0045661_regulation of myoblast differentiation	7	63	332	12262	12226;17260;17329;20307;57810;69564;319594	0.0026	0.0408	GOBP	mmu-miR-29a-3p
GO:0051893_regulation of focal adhesion assembly	6	57	332	12262	14260;19271;20874;22417;105352;110829	0.0066	0.0408	GOBP	mmu-miR-29a-3p
GO:0046782_regulation of viral transcription	5	41	332	12262	22695;98415;230908;233532;328572	0.0073	0.0408	GOBP	mmu-miR-29a-3p
GO:0006493_protein O-linked glycosylation	6	61	332	12262	14426;52463;97884;108155;214133;223827	0.0088	0.0408	GOBP	mmu-miR-29a-3p
GO:1903391_regulation of adherens junction organization	6	63	332	12262	14260;19271;20874;22417;105352;110829	0.0101	0.041	GOBP	mmu-miR-29a-3p
mmu04728_Dopaminergic_synapse	10	135	243	8275	12288;12753;14681;14688;14700;14701;14706;16522;53623;56637	0.0099	0.0413	KEGG	mmu-miR-342-3p
mmu04010_MAPK_signaling_pathway	17	294	243	8275	11600;12288;12298;13874;14175;14176;14701;16151;16180;16337;18015;18018;18021;18595;19419;20662;266632	0.0104	0.0415	KEGG	mmu-miR-342-3p
mmu04550_Signaling_pathways_regulating_pluripotency_of_stem_cells	10	137	243	8275	11480;16880;17126;17127;18710;21423;22658;56637;57265;76073	0.0108	0.0415	KEGG	mmu-miR-342-3p
mmu05215_Prostate_cancer	8	97	243	8275	16151;17395;18595;18607;18710;20662;21415;56637	0.0113	0.0417	KEGG	mmu-miR-342-3p
GO:0034333_adherens junction assembly	7	84	332	12262	14260;15257;19271;20874;22417;105352;110829	0.0109	0.0419	GOBP	mmu-miR-29a-3p
GO:0007044_cell-substrate junction assembly	7	85	332	12262	14260;16402;19271;20874;22417;105352;110829	0.0115	0.042	GOBP	mmu-miR-29a-3p
mmu04625_C-type_lectin_receptor_signaling_pathway	33	112	1369	8275	11651;11652;11848;12042;12313;12315;15461;16150;16151;16159;16362;170780;170786;18018;18176;18706;18708;18709;1871	0.004	0.0462	KEGG	mmu-miR-744-5p

					0;19059;20299;26413;26415;26416;26419;26420;53859;56489;66824;69142;69165;74256;74769				
mmu04211_Longevity_regulating_pathway	28	90	1369	8275	105787;108079;108097;11651;11652;11909;12028;13684;13685;15461;16000;16369;18176;18706;18708;18709;18710;19017;207565;218268;22059;231991;241113;56484;68465;72508;72674;74769	0.0041	0.0462	KEGG	mmu-miR-744-5p
mmu04071_Sphingolipid_signaling_pathway	35	122	1369	8275	11651;11652;11848;12028;12062;14678;15461;171168;18176;18386;18706;18708;18709;18710;18750;18754;18762;18796;18806;19054;19878;20397;22059;26413;26415;26416;26419;26420;26931;269643;54447;59032;67260;74442;74769	0.0044	0.0477	KEGG	mmu-miR-744-5p
GO:0048525_negative regulation of viral process	7	97	332	12262	17535;19130;22695;24014;230908;231699;246729	0.0213	0.049	GOBP	mmu-miR-29a-3p
GO:0031058_positive regulation of histone modification	7	97	332	12262	13163;20874;22083;22724;52463;108155;328572	0.0213	0.049	GOBP	mmu-miR-29a-3p
GO:0031016_pancreas development	7	89	332	12262	12571;12753;13666;15378;19130;19726;100039795	0.0143	0.049	GOBP	mmu-miR-29a-3p
GO:0002028_regulation of sodium ion transport	7	91	332	12262	16150;20720;83814;93692;94253;246198;329152	0.0159	0.049	GOBP	mmu-miR-29a-3p
GO:0001954_positive regulation of cell-matrix adhesion	5	52	332	12262	12571;14260;19271;22417;110829	0.0176	0.049	GOBP	mmu-miR-29a-3p
GO:0007045_cell-substrate adherens junction assembly	6	75	332	12262	14260;19271;20874;22417;105352;110829	0.021	0.049	GOBP	mmu-miR-29a-3p
GO:0070988_demethylation	5	53	332	12262	18676;52463;73945;214133;214899	0.0188	0.049	GOBP	mmu-miR-29a-3p
GO:0050732_negative regulation of peptidyl-tyrosine phosphorylation	5	55	332	12262	15378;16923;19255;28084;105352	0.0215	0.049	GOBP	mmu-miR-29a-3p
GO:0035967_cellular response to topologically incorrect protein	7	97	332	12262	13163;13666;19255;76867;77128;231630;328572	0.0213	0.049	GOBP	mmu-miR-29a-3p
GO:0031018_endocrine pancreas development	5	51	332	12262	12571;12753;13666;15378;19726	0.0164	0.049	GOBP	mmu-miR-29a-3p

GO:0048041_focal adhesion assembly	6	75	332	12262	14260;19271;20874;22417;105352;110829	0.021	0.049	GOBP	mmu-miR-29a-3p
GO:0060761_negative regulation of response to cytokine stimulus	5	53	332	12262	16923;19255;21906;23938;73945	0.0188	0.049	GOBP	mmu-miR-29a-3p
mmu05200_Pathways_in_cancer	26	530	243	8275	12395;14175;14176;14296;14688;14700;14701;14706;16151;16399;16410;17126;17127;17395;18595;18710;19206;19419;20662;212398;21415;235320;23871;53978;56637;57265	0.0138	0.0491	KEGG	mmu-miR-342-3p
mmu04933_AGE-RAGE_signaling_pathway_in_diabetic_complications	30	100	1369	8275	11651;11652;12028;12367;12443;12576;15461;17126;17127;18018;18176;18706;18708;18709;18710;18750;18754;18762;18796;18802;20851;21824;26413;26415;26416;26419;26420;50490;74055;74769	0.0047	0.0491	KEGG	mmu-miR-744-5p
mmu05215_Prostate_cancer	29	97	1369	8275	109880;11651;11652;11835;12371;12387;12443;12576;14182;14784;15461;16000;16150;16151;18095;18176;18591;18596;18706;18708;18709;18710;21802;22059;231991;26413;50528;56637;74769	0.0056	0.0494	KEGG	mmu-miR-744-5p
mmu05223_Non-small_cell_lung_cancer	22	66	1369	8275	109880;11651;11652;12028;12371;12443;12571;14784;15461;18176;18706;18708;18709;18710;18750;20851;21802;22059;26413;56484;58231;74769	0.0053	0.0494	KEGG	mmu-miR-744-5p
mmu05100_Bacterial_invasion_of_epithelial_cells	24	74	1369	8275	11848;12387;12928;12929;13043;13430;140580;18000;18706;18708;18709;18710;19303;20416;216033;216148;234683;271849;330662;52398;56526;71089;74325;74769	0.0049	0.0494	KEGG	mmu-miR-744-5p
mmu05212_Pancreatic_cancer	24	75	1369	8275	109880;11651;11652;12028;12371;12443;12571;16150;16151;17126;17127;18706;18708;18709;18710;19765;21802;22059;26413;26419;26420;72508;73341;74769	0.0056	0.0494	KEGG	mmu-miR-744-5p
mmu05213_Endometrial_cancer	20	58	1369	8275	109880;11651;11652;12028;12371;12387;12443;14784;15461;18176;18706;18708;18709;18710;216033;22059;26413;56484;56637;74769	0.0056	0.0494	KEGG	mmu-miR-744-5p

Supplementary Table 2

Name	Hits	Pop Hits	List Total	Pop Total	Genes	Pvalue	adjusted Pvalue (BH)	Ontology	MicroRNA
mmu04012_ErbB_signaling_pathway	10	84	153	8275	Erbb4;Abl2;Pik3ca;Nras;Camk2d;Braf;Prkcb;Map2k7;Map2k4;Pik3r1	0	0	KEGG	mmu-miR-192-5p
mmu04071_Sphingolipid_signaling_pathway	9	122	153	8275	Sgpp2;Pik3ca;Nras;Gnai3;Oprd1;Prkcb;S1pr2;Sptlc2;Pik3r1	0.0008	0.0166	KEGG	mmu-miR-192-5p
mmu05214_Glioma	7	71	153	8275	Pik3ca;Nras;Camk2d;E2f2;Braf;Prkcb;Pik3r1	0.0006	0.0166	KEGG	mmu-miR-192-5p
mmu04360_Axon_guidance	11	175	153	8275	Enah;Pik3ca;Nras;Gnai3;Camk2d;Epha7;Smo;Plxna4;Arhgef12;Efna2;Pik3r1	0.0008	0.0166	KEGG	mmu-miR-192-5p
GO:0046854_phosphatidylinositol phosphorylation	5	38	261	12262	Bpnt1;Pik3ca;Fam126a;Pik3r1;Pi4k2a	0.002	0.0225	GOBP	mmu-miR-192-5p
GO:0046834_lipid phosphorylation	6	49	261	12262	Bpnt1;Pik3ca;Fam126a;Pik3r1;Dgkh;Pi4k2a	0.001	0.0225	GOBP	mmu-miR-192-5p
GO:0000266_mitochondrial fission	5	40	261	12262	Mfn1;Mul1;Mtfr2;Ddhd1;Slc25a46	0.0025	0.0225	GOBP	mmu-miR-192-5p
GO:0055013_cardiac muscle cell development	8	99	261	12262	Hnrnpu;Camk2d;Xirp1;Map2k4;Ppara;Cxadr;Slc8a1;Prkg1	0.002	0.0225	GOBP	mmu-miR-192-5p
GO:0010389_regulation of G2/M transition of mitotic cell cycle	7	78	261	12262	Pbx1;Camk2d;Atm;Cdk1;Hus1;Cdc6;Rad51b	0.0022	0.0225	GOBP	mmu-miR-192-5p
GO:0040018_positive regulation of multicellular organism growth	5	43	261	12262	Celf1;Sgip1;Smo;Igf2;Tshr	0.0033	0.0248	GOBP	mmu-miR-192-5p
GO:1904705_regulation of vascular smooth muscle cell proliferation	5	53	261	12262	Rgs5;Gnai3;Camk2d;Ldlrap1;Prkg1	0.0075	0.0281	GOBP	mmu-miR-192-5p
GO:0060043_regulation of cardiac muscle cell proliferation	5	50	261	12262	Erbb4;Yap1;Cdk1;Jarid2;Cxadr	0.006	0.0281	GOBP	mmu-miR-192-5p
GO:1901989_positive regulation of cell cycle phase transition	7	96	261	12262	Cul3;Pbx1;Camk2d;Cdk1;Lsm11;Stxbp4;Rad51b	0.0063	0.0281	GOBP	mmu-miR-192-5p
GO:1902749_regulation of cell cycle G2/M phase transition	7	94	261	12262	Pbx1;Camk2d;Atm;Cdk1;Hus1;Cdc6;Rad51b	0.0057	0.0281	GOBP	mmu-miR-192-5p
GO:1990874_vascular smooth muscle	5	53	261	12262	Rgs5;Gnai3;Camk2d;Ldlrap1;Prkg1	0.0075	0.0281	GOBP	mmu-miR-

cell proliferation									192-5p
GO:0042102_positive regulation of T cell proliferation	7	98	261	12262	Cd46;Il21;Ceacam1;Igf2;Icosl;Havcr2;Tnfrsf13c	0.007	0.0281	GOBP	mmu-miR-192-5p
GO:0055021_regulation of cardiac muscle tissue growth	6	77	261	12262	Erbb4;Yap1;Cdk1;Jarid2;Ppara;Cxadr	0.0083	0.0287	GOBP	mmu-miR-192-5p
GO:0044774_mitotic DNA integrity checkpoint	5	64	261	12262	Atm;Cdk1;Hus1;Cdc6;Ppp1r10	0.0152	0.0326	GOBP	mmu-miR-192-5p
GO:0060038_cardiac muscle cell proliferation	5	62	261	12262	Erbb4;Yap1;Cdk1;Jarid2;Cxadr	0.0135	0.0326	GOBP	mmu-miR-192-5p
GO:1904356_regulation of telomere maintenance via telomere lengthening	5	62	261	12262	Hnrnpu;Nek2;Map2k7;Atm;Ercc4	0.0135	0.0326	GOBP	mmu-miR-192-5p
GO:0032204_regulation of telomere maintenance	6	82	261	12262	Hnrnpu;Nek2;Map2k7;Atm;Ercc4;Ppp1r10	0.0109	0.0326	GOBP	mmu-miR-192-5p
GO:2000736_regulation of stem cell differentiation	5	63	261	12262	Hnrnpu;N4bp2l2;Yap1;Prickle1;Eif2ak2	0.0143	0.0326	GOBP	mmu-miR-192-5p
GO:0071479_cellular response to ionizing radiation	5	64	261	12262	Rad51ap1;Yap1;Atm;Hus1;Net1	0.0152	0.0326	GOBP	mmu-miR-192-5p
GO:0060420_regulation of heart growth	6	84	261	12262	Erbb4;Yap1;Cdk1;Jarid2;Ppara;Cxadr	0.012	0.0326	GOBP	mmu-miR-192-5p
GO:1901992_positive regulation of mitotic cell cycle phase transition	6	83	261	12262	Cul3;Pbx1;Camk2d;Cdk1;Lsm11;Rad51b	0.0114	0.0326	GOBP	mmu-miR-192-5p
GO:0040014_regulation of multicellular organism growth	6	90	261	12262	Celf1;Pik3ca;Sgip1;Smo;Igf2;Tshr	0.0161	0.0329	GOBP	mmu-miR-192-5p
GO:0032922_circadian regulation of gene expression	5	66	261	12262	Hnrnpu;Top1;Gfpt1;Rora;Ppara	0.017	0.0333	GOBP	mmu-miR-192-5p
GO:0034109_homotypic cell-cell adhesion	5	68	261	12262	Slc7a11;Ceacam1;Ubash3b;Cxadr;Prkg1	0.0189	0.0354	GOBP	mmu-miR-192-5p
mmu05223_Non-small_cell_lung_cancer	6	66	153	8275	Pik3ca;Nras;E2f2;Braf;Prkcb;Pik3r1	0.0022	0.0365	KEGG	mmu-miR-192-5p
GO:2001021_negative regulation of response to DNA damage stimulus	5	70	261	12262	Trim32;3110062M04Rik;Mb21d1;Ercc4;Ppp1r10	0.021	0.0378	GOBP	mmu-miR-192-5p
GO:0048525_negative regulation of viral process	6	97	261	12262	Trim32;Tardbp;Ceacam1;Pou2f3;Rsad2;Eif2ak2	0.022	0.0381	GOBP	mmu-miR-192-5p
GO:0090174_organelle membrane fusion	6	100	261	12262	Vps39;Mfn1;Gnai3;Syt9;Sept8;Stx8	0.0249	0.0413	GOBP	mmu-miR-192-5p

GO:0010822_positive regulation of mitochondrion organization	5	74	261	12262	Mfn1;Mul1;Smurf1;Ddhd1;Pmaip1	0.0257	0.0413	GOBP	mmu-miR-192-5p
GO:0010833_telomere maintenance via telomere lengthening	5	76	261	12262	Hnrnpu;Nek2;Map2k7;Atm;Ercc4	0.0282	0.0415	GOBP	mmu-miR-192-5p
GO:0032729_positive regulation of interferon-gamma production	5	77	261	12262	Abl2;Il21;Nras;Havcr2;Tnfrsf13c	0.0295	0.0415	GOBP	mmu-miR-192-5p
GO:1900182_positive regulation of protein localization to nucleus	5	75	261	12262	Tardbp;Smo;Cdk1;Pik3r1;Glis2	0.0269	0.0415	GOBP	mmu-miR-192-5p
GO:0014855_striated muscle cell proliferation	5	77	261	12262	Erbb4;Yap1;Cdk1;Jarid2;Cxadr	0.0295	0.0415	GOBP	mmu-miR-192-5p
mmu04725_Cholinergic_synapse	7	113	153	8275	Kcnq2;Pik3ca;Nras;Gnai3;Camk2d;Prkcb;Pik3r1	0.0072	0.042	KEGG	mmu-miR-192-5p
mmu05225_Hepatocellular_carcinoma	9	171	153	8275	Pik3ca;Nras;E2f2;Braf;Prkcb;Igf2;Tcf7;Pik3r1;Frat1	0.0068	0.042	KEGG	mmu-miR-192-5p
mmu05213_Endometrial_cancer	5	58	153	8275	Pik3ca;Nras;Braf;Tcf7;Pik3r1	0.0062	0.042	KEGG	mmu-miR-192-5p
mmu04931_Insulin_resistance	7	109	153	8275	Prkag3;Pik3ca;Prkab2;Gfpt1;Prkcb;Pik3r1;Ppara	0.006	0.042	KEGG	mmu-miR-192-5p
mmu04068_FoxO_signaling_pathway	8	132	153	8275	Prkag3;Pik3ca;Prkab2;Nras;Braf;Atm;Agap2;Pik3r1	0.0048	0.042	KEGG	mmu-miR-192-5p
mmu04210_Apoptosis	8	136	153	8275	Pik3ca;Nras;Atm;Map3k14;Pik3r1;Csf2rb;Pmaip1;Ctsf	0.0057	0.042	KEGG	mmu-miR-192-5p
mmu05205_Proteoglycans_in_cancer	10	204	153	8275	Erbb4;Pik3ca;Nras;Camk2d;Smo;Braf;Prkcb;Igf2;Arhgef12;Pik3r1	0.0072	0.042	KEGG	mmu-miR-192-5p
mmu04923_Regulation_of_lipolysis_in_adipocytes	5	55	153	8275	Pik3ca;Gnai3;Tshr;Pik3r1;Prkg1	0.005	0.042	KEGG	mmu-miR-192-5p
mmu04730_Long-term_depression	5	61	153	8275	Nras;Gnai3;Braf;Prkcb;Prkg1	0.0075	0.042	KEGG	mmu-miR-192-5p
mmu04213_Longevity_regulating_pathway	5	62	153	8275	Prkag3;Pik3ca;Prkab2;Nras;Pik3r1	0.008	0.042	KEGG	mmu-miR-192-5p
mmu05210_Colorectal_cancer	6	88	153	8275	Pik3ca;Nras;Braf;Tcf7;Pik3r1;Pmaip1	0.0081	0.042	KEGG	mmu-miR-192-5p
GO:0043525_positive regulation of neuron apoptotic process	5	79	261	12262	Epha7;Map2k7;Atm;Map2k4;Pmaip1	0.0323	0.0428	GOBP	mmu-miR-192-5p
GO:0050805_negative regulation of synaptic transmission	5	79	261	12262	Braf;S1pr2;Arf1;Pcdh17;Sorcs3	0.0323	0.0428	GOBP	mmu-miR-192-5p

Supplementary Table 3

Name	Hits	Pop Hits	List Total	Pop Total	Genes	Pvalue	adjusted Pvalue (BH)	Ontology	MicroRNA
mmu04012_ErbB_signaling_pathway	10	84	153	8275	Erbb4;Abl2;Pik3ca;Nras;Camk2d;Braf;Prkcb;Map2k7;Map2k4;Pik3r1	0	0	KEGG	mmu-miR-192-5p
mmu05226_Gastric_cancer	34	150	777	8275	Bcl2;Akt3;E2f1;Pik3ca;Wnt2b;Cdh17;Tgfbr1;Fzd1;Fzd9;Wnt2;Braf;Ctnna2;Fgf23;Ccne1;Bax;Ccnd1;Apc2;Map2k2;Tcf7;Wnt9a;Jup;Tgfb3;E2f3;Wnt5a;Fzd3;Wnt1;Cdkn1a;Rxrb;Sos1;Fgf1;Smad2;Frat1;Araf;Fgf16	0	0	KEGG	mmu-miR-345-5p
mmu05200_Pathways_in_cancer	86	530	777	8275	Tceb1;Bcl2;Rassf5;Lamc2;Akt3;Traf1;Spi1;Bcl2l11;Jag1;E2f1;Hey1;Pik3ca;Tpm3;Arnt;Wnt2b;Runx1t1;Tgfbr1;Lpar1;Casp9;Plekhg5;Cdk6;Fzd1;Mapk10;Fzd9;Wnt2;Braf;Gng12;Ctnna2;Cxcl12;Bid;Fgf23;Calm3;Ccne1;Bax;Igf1r;Arnt2;Il4ra;Igf2;Ccnd1;Egln1;Arhgef12;Zbtb16;Esr1;Lama4;Ccdc6;Apc2;Map2k2;Txnrd1;Kitl;Stat6;Camk2b;Tcf7;Il13;Wnt9a;Crk;Traf4;Jup;Birc5;Adcy3;Tgfb3;Calm1;Calml3;E2f3;Il6st;Il3ra;Gng2;Wnt5a;Fzd3;Wnt1;Ifnar2;Cdkn1a;Rxrb;Sos1;Cul2;Rock1;Fgf1;Camk2a;Pdgfrb;Pmaip1;Smad2;Plcb3;Frat1;Pim2;Araf;Ikbkg;Fgf16	0	0	KEGG	mmu-miR-345-5p
mmu04152_AMPK_signaling_pathway	29	126	777	8275	Creb1;Pfkfb2;Adipor1;Akt3;Pfkfb3;Rab14;Hnf4a;Pik3ca;Ccna2;Pr	0.0001	0.0056	KEGG	mmu-miR-345-5p

					kag2;Ppp2r2c;Tbc1d1;Prkab1;Lep;Creb3l2;Igf1r;Ccnd1;Foxo3;Slc2a4;Ppp2r3c;Ppp2r5c;Hmgcr;Ppp2r2a;Prkaa1;Cpt1b;Pdpk1;Ppp2r5d;Cpt1a;Scd1				
mmu05224_Breast_cancer	31	147	777	8275	Akt3;Jag1;E2f1;Hey1;Pik3ca;Wnt2b;Cdk6;Fzd1;Fzd9;Wnt2;Braf;Fgf23;Bax;Igf1r;Ccnd1;Esr1;Apc2;Map2k2;Tcf7;Wnt9a;E2f3;Wnt5a;Fzd3;Tnfsf11;Wnt1;Cdkn1a;Sos1;Fgf1;Frat1;Araf;Fgf16	0.0001	0.0056	KEGG	mmu-miR-345-5p
mmu04071_Sphingolipid_signaling_pathway	27	122	777	8275	Sgpp2;Bcl2;Akt3;Degs1;Pik3ca;Adora3;Ppp2r2c;Mapk10;Bid;Bax;Cers3;Gab2;Cers4;S1pr2;Sgpl1;Map2k2;S1pr4;Ppp2r3c;Ppp2r5c;Sptlc1;Ppp2r2a;Abcc1;Pdpk1;Ppp2r5d;Prkce;Rock1;Plcb3	0.0002	0.0075	KEGG	mmu-miR-345-5p
mmu05214_Glioma	19	71	777	8275	Akt3;E2f1;Pik3ca;Cdk6;Braf;Calm3;Bax;Igf1r;Ccnd1;Map2k2;Camk2b;Calm1;Calml3;E2f3;Cdkn1a;Sos1;Camk2a;Pdgfrb;Araf	0.0002	0.0075	KEGG	mmu-miR-345-5p
mmu04261_Adrenergic_signaling_in_cardiomyocytes	30	147	777	8275	Creb1;Bcl2;Atp2b4;Atp1b1;Akt3;Adra1d;Tpm3;Tpm2;Ppp2r2c;Creb3l2;Cacna2d4;Cacng7;Calm3;Tpm4;Tpm1;Camk2b;Adcy3;Pik3cg;Ppp2r3c;Calm1;Ppp2r5c;Calml3;Ppp2r2a;Cacnb3;Atf6b;Ppp2r5d;Camk2a;Plcb3;Atp1b4;Atp2b3	0.0003	0.0084	KEGG	mmu-miR-345-5p
mmu05205_Proteoglycans_in_cancer	38	204	777	8275	Erbb4;Akt3;Src;Pik3ca;Wnt2b;Tlr4;Fzd1;Hpse;Pxn;Fzd9;Wnt2;Braf;Itpr2;Plaur;Igf1r;Igf2;Cttn;Ccnd1;Arhgef12;Rdx;Mras;Esr1;Map2k2;Camk2b;Wnt9a;Ctsl;Wnt5a;Fzd3;Wnt1;Eif4b;Pdpk1;Cdkn1a;Sos1;Rock1;Hbegf;Camk2a;Smad2;Araf	0.0003	0.0084	KEGG	mmu-miR-345-5p

mmu04934_Cushing_syndrome	31	158	777	8275	Creb1;Kcnk2;E2f1;Nceh1;Arnt;Wnt2b;Cdk6;Fzd1;Fzd9;Wnt2;Creb3l2;Braf;Itpr2;Ccne1;Ccnd1;Star;Apc2;Map2k2;Camk2b;Tcf7;Wnt9a;Adcy3;E2f3;Wnt5a;Fzd3;Cacna1i;Wnt1;Cdkn1a;Atf6b;Camk2a;Plcb3	0.0004	0.009	KEGG	mmu-miR-345-5p
mmu05161_Hepatitis_B	29	143	777	8275	Creb1;Bcl2;Akt3;Mavs;E2f1;Src;Pik3ca;Ccna2;Tgfbr1;Tlr4;Casp9;Cdk6;Mapk10;Creb3l2;Ccne1;Bax;Ccnd1;Tirap;Egr2;Map2k2;Stat6;Map2k4;Birc5;Tgfb3;E2f3;Ywhaz;Cdkn1a;Atf6b;Ikbkg	0.0004	0.009	KEGG	mmu-miR-345-5p
mmu05223_Non-small_cell_lung_cancer	17	66	777	8275	Rassf5;Akt3;E2f1;Pik3ca;Casp9;Cdk6;Braf;Bax;Ccnd1;Foxo3;Map2k2;E2f3;Pdpk1;Cdkn1a;Rxrb;Sos1;Araf	0.0007	0.0131	KEGG	mmu-miR-345-5p
mmu05225_Hepatocellular_carcinoma	32	171	777	8275	Akt3;E2f1;Pik3ca;Actl6a;Wnt2b;Tgfbr1;Cdk6;Fzd1;Fzd9;Wnt2;Braf;Dpf1;Bax;Igf1r;Igf2;Ccnd1;Apc2;Map2k2;Txnrd1;Tcf7;Wnt9a;Smarcd2;Tgfb3;E2f3;Wnt5a;Fzd3;Wnt1;Cdkn1a;Sos1;Smad2;Frat1;Araf	0.0007	0.0131	KEGG	mmu-miR-345-5p
mmu04928_Parathyroid_hormone_synthesis,_secretion_and_action	23	107	777	8275	Creb1;Bcl2;Mmp16;Creb3l2;Braf;Fgf23;Itpr2;Mef2a;Arrb1;Mmp15;Pde4a;Pth1r;Adcy3;Mmp14;Tnfsf11;Vdr;Cdkn1a;Rxrb;Atf6b;Runx2;Hbegf;Plcb3;Araf	0.0008	0.0138	KEGG	mmu-miR-345-5p
mmu05210_Colorectal_cancer	20	88	777	8275	Bcl2;Akt3;Bcl2l11;Pik3ca;Tgfbr1;Casp9;Mapk10;Braf;Bax;Ccnd1;Apc2;Map2k2;Tcf7;Birc5;Tgfb3;Cdkn1a;Sos1;Pmaip1;Smad2;Araf	0.0009	0.0144	KEGG	mmu-miR-345-5p
mmu04151_PI3K-Akt_signaling_pathway	55	358	777	8275	Creb1;Erbb4;Eif4e2;Bcl2;Lamc2;Akt3;Bcl2l11;Col9a3;Pik3ca;Lpar	0.0011	0.0164	KEGG	mmu-miR-345-5p

					1;Tlr4;Epha2;Casp9;Cdk6;Ppp2r2c;Creb3l2;Gng12;Magi1;Fgf23;Ccne1;Igf1r;Il4ra;Igf2;Ccnd1;Itga11;Lama4;Foxo3;Col6a2;Map2k2;Kitl;Ngfr;Csf3;Pik3cg;Ppp2r3c;Ppp2r5c;Ntrk2;Il3ra;Gng2;Ppp2r2a;Prkaa1;Osmr;Ywhaz;Eif4b;Ifnar2;Pdpk1;Cdkn1a;Atf6b;Ppp2r5d;Efna5;Sos1;Fgf1;Pdgfrb;Ikbkg;Mtcp1;Fgf16				
mmu04071_Sphingolipid_signaling_pathway	9	122	153	8275	Sgpp2;Pik3ca;Nras;Gnai3;Oprd1;Prkcb;S1pr2;Sptlc2;Pik3r1	0.0008	0.0166	KEGG	mmu-miR-192-5p
mmu05214_Glioma	7	71	153	8275	Pik3ca;Nras;Camk2d;E2f2;Braf;Prkcb;Pik3r1	0.0006	0.0166	KEGG	mmu-miR-192-5p
mmu04360_Axon_guidance	11	175	153	8275	Enah;Pik3ca;Nras;Gnai3;Camk2d;Epha7;Smo;Plxna4;Arhgef12;Efna2;Pik3r1	0.0008	0.0166	KEGG	mmu-miR-192-5p
mmu05213_Endometrial_cancer	15	58	777	8275	Akt3;Pik3ca;Casp9;Braf;Ctnna2;Bax;Ccnd1;Foxo3;Apc2;Map2k2;Tcf7;Pdpk1;Cdkn1a;Sos1;Araf	0.0013	0.0182	KEGG	mmu-miR-345-5p
GO:0090398_cellular senescence	6	63	240	12262	Slc30a10;Pla2r1;Prmt6;Wnt16;Arntl;Hmga2	0.0023	0.0186	GOBP	mmu-miR-21a-5p
GO:0032922_circadian regulation of gene expression	6	66	240	12262	Ncoa2;Per2;Arntl;Rora;Ppara;Huwe1	0.0028	0.0186	GOBP	mmu-miR-21a-5p
GO:0048864_stem cell development	7	91	240	12262	Erbb4;Gbx2;Klhl12;Jag1;Sema3e;Sema5a;Wnt7b	0.0031	0.0186	GOBP	mmu-miR-21a-5p
GO:0070542_response to fatty acid	5	51	240	12262	Pid1;Tlr4;Foxp1;Ptgdr;Scd4	0.0046	0.0207	GOBP	mmu-miR-21a-5p
mmu04360_Axon_guidance	36	175	768	8275	Sema4c;Enah;Pdk1;Nfatc2;Sema6c;Pik3r3;Ephb2;Pik3cd;Prkcz;Cdk5;Dpysl5;Limk1;Lrrc4;Plxna4;Plxna1;Srgap3;Sema7a;Rhoa;Fyn;Unc5b;Ppp3r1;Ntn1;Ssh2;Prkca;Rock2;Pik3r1;Nfatc4;Dpysl2;Rnd1;Ephb3;Pak2;Gsk3b;Sema6a;Camk2a;Pard6g;Ablim1	0.0001	0.021	KEGG	mmu-miR-150-5p

mmu04916_Melanogenesis	21	100	777	8275	Creb1;Wnt2b;Fzd1;Fzd9;Wnt2;Creb3l2;Calm3;Gnao1;Map2k2;Kitl;Camk2b;Tcf7;Wnt9a;Adcy3;Calm1;Calml3;Wnt5a;Fzd3;Wnt1;Camk2a;Plcb3	0.0016	0.0211	KEGG	mmu-miR-345-5p
GO:0046854_phosphatidylinositol phosphorylation	5	38	261	12262	Bpnt1;Pik3ca;Fam126a;Pik3r1;Pi4k2a	0.002	0.0225	GOBP	mmu-miR-192-5p
GO:0046834_lipid phosphorylation	6	49	261	12262	Bpnt1;Pik3ca;Fam126a;Pik3r1;Dgkh;Pi4k2a	0.001	0.0225	GOBP	mmu-miR-192-5p
GO:0000266_mitochondrial fission	5	40	261	12262	Mfn1;Mul1;Mtfr2;Ddhd1;Slc25a46	0.0025	0.0225	GOBP	mmu-miR-192-5p
GO:0055013_cardiac muscle cell development	8	99	261	12262	Hnrnpu;Camk2d;Xirp1;Map2k4;Ppara;Cxadr;Slc8a1;Prkg1	0.002	0.0225	GOBP	mmu-miR-192-5p
GO:0010389_regulation of G2/M transition of mitotic cell cycle	7	78	261	12262	Pbx1;Camk2d;Atm;Cdk1;Hus1;Cdc6;Rad51b	0.0022	0.0225	GOBP	mmu-miR-192-5p
mmu04022_cGMP-PKG_signaling_pathway	30	168	777	8275	Creb1;Atp2b4;Atp1b1;Akt3;Adra2b;Adra1d;Adora3;Pde5a;Ppp3r2;Gtf2i;Creb3l2;Itpr2;Calm3;Mef2a;Cngb1;Map2k2;Kcnmb4;Ppp3r1;Kcnmb1;Adcy3;Pik3cg;Calm1;Calml3;Atf6b;Prkce;Rock1;Plcb3;Prkg1;Atp1b4;Atp2b3	0.0019	0.0236	KEGG	mmu-miR-345-5p
GO:0016239_positive regulation of macroautophagy	5	67	240	12262	Gpsm1;Lrsam1;Map3k7;Rab12;Ikbkg	0.0131	0.0242	GOBP	mmu-miR-21a-5p
GO:0014031_mesenchymal cell development	6	90	240	12262	Erbb4;Gbx2;Klhl12;Jag1;Sema3e;Sema5a	0.0112	0.0242	GOBP	mmu-miR-21a-5p
GO:0002702_positive regulation of production of molecular mediator of immune response	6	100	240	12262	Arid5a;Cd244;Tlr4;Whsc1;Foxp1;Il33	0.0175	0.0242	GOBP	mmu-miR-21a-5p
GO:0014032_neural crest cell development	6	85	240	12262	Erbb4;Gbx2;Klhl12;Jag1;Sema3e;Sema5a	0.0088	0.0242	GOBP	mmu-miR-21a-5p
GO:0010771_negative regulation of cell morphogenesis involved in differentiation	6	99	240	12262	Draxin;Sema3e;Trpc6;Ryk;Sema5a;Pten	0.0168	0.0242	GOBP	mmu-miR-21a-5p
GO:0014033_neural crest cell differentiation	6	92	240	12262	Erbb4;Gbx2;Klhl12;Jag1;Sema3e;Sema5a	0.0123	0.0242	GOBP	mmu-miR-21a-5p

GO:0001578_microtubule bundle formation	6	99	240	12262	Clasp1;Chp1;Tppp;Ccdc66;Ccser2;Iqcg	0.0168	0.0242	GOBP	mmu-miR-21a-5p
GO:0032482_Rab protein signal transduction	5	68	240	12262	Rab38;Rab11a;Rab1a;Rab2b;Rab12	0.0138	0.0242	GOBP	mmu-miR-21a-5p
GO:0050771_negative regulation of axonogenesis	5	67	240	12262	Draxin;Sema3e;Ryk;Sema5a;Pten	0.0131	0.0242	GOBP	mmu-miR-21a-5p
GO:0040018_positive regulation of multicellular organism growth	5	43	261	12262	Celf1;Sgip1;Smo;Igf2;Tshr	0.0033	0.0248	GOBP	mmu-miR-192-5p
mmu04390_Hippo_signaling_pathway	28	154	777	8275	Trp53bp2;Wnt2b;Tgfbr1;Fzd1;Ppp2r2c;Fzd9;Serpine1;Wnt2;Ctnna2;Dlg2;Tead1;Ccnd1;Limd1;Apc2;Fbxw11;Tcf7;Wnt9a;Birc5;Mpp5;Tgfb3;Wnt5a;Fzd3;Ppp2r2a;Ywhaz;Wnt1;Fgf1;Smad2;Amot	0.0021	0.0248	KEGG	mmu-miR-345-5p
mmu05221_Acute_myeloid_leukemia	16	69	777	8275	Per2;Akt3;Spi1;Pik3ca;Fcgr1;Runx1t1;Braf;Ccnd1;Zbtb16;Map2k2;Tcf7;Jup;Sos1;Pim2;Araf;Ikbkg	0.0023	0.0255	KEGG	mmu-miR-345-5p
mmu05220_Chronic_myeloid_leukemia	17	76	777	8275	Akt3;E2f1;Pik3ca;Tgfbr1;Cdk6;Braf;Bax;Gab2;Ccnd1;Map2k2;Crk;Tgfb3;E2f3;Cdkn1a;Sos1;Araf;Ikbkg	0.0024	0.0255	KEGG	mmu-miR-345-5p
mmu05215_Prostate_cancer	20	97	777	8275	Creb1;Bcl2;Akt3;E2f1;Pik3ca;Casp9;Creb3l2;Braf;Ccne1;Igf1r;Ccnd1;Map2k2;Tcf7;E2f3;Pdpk1;Cdkn1a;Sos1;Pdgfrb;Araf;Ikbkg	0.0025	0.0255	KEGG	mmu-miR-345-5p
GO:1904705_regulation of vascular smooth muscle cell proliferation	5	53	261	12262	Rgs5;Gnai3;Camk2d;Ldlrap1;Prkg1	0.0075	0.0281	GOBP	mmu-miR-192-5p
GO:0060043_regulation of cardiac muscle cell proliferation	5	50	261	12262	Erbb4;Yap1;Cdk1;Jarid2;Cxadr	0.006	0.0281	GOBP	mmu-miR-192-5p
GO:1901989_positive regulation of cell cycle phase transition	7	96	261	12262	Cul3;Pbx1;Camk2d;Cdk1;Lsm11;Stxbp4;Rad51b	0.0063	0.0281	GOBP	mmu-miR-192-5p
GO:1902749_regulation of cell cycle G2/M phase transition	7	94	261	12262	Pbx1;Camk2d;Atm;Cdk1;Hus1;Cdc6;Rad51b	0.0057	0.0281	GOBP	mmu-miR-192-5p
GO:1990874_vascular smooth muscle cell proliferation	5	53	261	12262	Rgs5;Gnai3;Camk2d;Ldlrap1;Prkg1	0.0075	0.0281	GOBP	mmu-miR-192-5p

GO:0042102_positive regulation of T cell proliferation	7	98	261	12262	Cd46;Il21;Ceacam1;Igf2;Icosl;Havcr2;Tnfrsf13c	0.007	0.0281	GOBP	mmu-miR-192-5p
GO:0055021_regulation of cardiac muscle tissue growth	6	77	261	12262	Erbb4;Yap1;Cdk1;Jarid2;Ppara;Cxadr	0.0083	0.0287	GOBP	mmu-miR-192-5p
GO:0033143_regulation of intracellular steroid hormone receptor signaling pathway	5	79	240	12262	Ncoa2;Arntl;Hmga2;Ddx5;Ntrk2	0.0239	0.0307	GOBP	mmu-miR-21a-5p
mmu04921_Oxytocin_signaling_pathway	27	153	777	8275	Kcnj9;Src;Ppp3r2;Prkag2;Cd38;Prkab1;Cacna2d4;Itpr2;Cacng7;Calm3;Ccnd1;Gnao1;Map2k2;Camk2b;Ppp3r1;Adcy3;Pik3cg;Calm1;Calml3;Prkaa1;Cacnb3;Rcan1;Kcnj6;Cdkn1a;Rock1;Camk2a;Plcb3	0.0036	0.031	KEGG	mmu-miR-345-5p
mmu01522_Endocrine_resistance	19	93	777	8275	Bcl2;Akt3;Jag1;E2f1;Src;Pik3ca;Mapk10;Braf;Bax;Igf1r;Ccnd1;Esr1;Map2k2;Adcy3;E2f3;Cdkn1a;Sos1;Hbegf;Araf	0.0034	0.031	KEGG	mmu-miR-345-5p
mmu05218_Melanoma	16	72	777	8275	Akt3;E2f1;Pik3ca;Cdk6;Braf;Fgf23;Bax;Igf1r;Ccnd1;Map2k2;E2f3;Cdkn1a;Fgf1;Pdgfrb;Araf;Fgf16	0.0034	0.031	KEGG	mmu-miR-345-5p
mmu04020_Calcium_signaling_pathway	31	184	777	8275	Erbb4;Avpr1b;Atp2b4;Grin1;Pde1a;Adra1d;Ntsr1;Ptgfr;Ppp3r2;Ptafr;Htr6;Cd38;P2rx7;Pde1c;Tacr1;Itpr2;Calm3;Grm5;Camk2b;Ppp3r1;P2rx5;Adcy3;Calm1;Calml3;Cacna1i;Camk2a;Pdgfrb;Plcb3;Atp2b3;Phka1;Cysltr1	0.0035	0.031	KEGG	mmu-miR-345-5p
mmu04020_Calcium_signaling_pathway	35	184	768	8275	Erbb4;Atp2b4;Itpkb;P2rx3;Gnas;Ptafr;Pdgfra;P2rx7;P2rx4;Orai2;Pde1c;Atp2b2;Grm5;Stim1;Orai3;Phkb;Avpr1a;Adcy1;Egfr;Ppp3r1;Adra1b;Vdac1;Cacna1g;Plcd3;Prkca;Grin2c;Chrm3;Adra1a;Cacna1i;P2rx6;Slc8a1;Camk2a;Pdgfrb;Htr4;Adrb1	0.0003	0.0315	KEGG	mmu-miR-150-5p

mmu04922_Glucagon_signaling_pathway	20	102	777	8275	Creb1;Akt3;Ppp3r2;Prkag2;Prkab1;Creb3l2;Itpr2;Calm3;Sik2;Gck;Camk2b;Ppp3r1;Calm1;Calml3;Prkaa1;Cpt1b;Camk2a;Cpt1a;Plcb3;Phka1	0.004	0.032	KEGG	mmu-miR-345-5p
mmu00900_Terpenoid_backbone_biosynthesis	8	23	777	8275	Icmt;Pcyox1;Acat1;Pdss2;Fntb;Hmgcr;Hmgcs1;Rce1	0.0039	0.032	KEGG	mmu-miR-345-5p
GO:0044774_mitotic DNA integrity checkpoint	5	64	261	12262	Atm;Cdk1;Hus1;Cdc6;Ppp1r10	0.0152	0.0326	GOBP	mmu-miR-192-5p
GO:0060038_cardiac muscle cell proliferation	5	62	261	12262	Erbb4;Yap1;Cdk1;Jarid2;Cxadr	0.0135	0.0326	GOBP	mmu-miR-192-5p
GO:1904356_regulation of telomere maintenance via telomere lengthening	5	62	261	12262	Hnrnpu;Nek2;Map2k7;Atm;Ercc4	0.0135	0.0326	GOBP	mmu-miR-192-5p
GO:0032204_regulation of telomere maintenance	6	82	261	12262	Hnrnpu;Nek2;Map2k7;Atm;Ercc4;Ppp1r10	0.0109	0.0326	GOBP	mmu-miR-192-5p
GO:2000736_regulation of stem cell differentiation	5	63	261	12262	Hnrnpu;N4bp2l2;Yap1;Prickle1;Eif2ak2	0.0143	0.0326	GOBP	mmu-miR-192-5p
GO:0071479_cellular response to ionizing radiation	5	64	261	12262	Rad51ap1;Yap1;Atm;Hus1;Net1	0.0152	0.0326	GOBP	mmu-miR-192-5p
GO:0060420_regulation of heart growth	6	84	261	12262	Erbb4;Yap1;Cdk1;Jarid2;Ppara;Cxadr	0.012	0.0326	GOBP	mmu-miR-192-5p
GO:1901992_positive regulation of mitotic cell cycle phase transition	6	83	261	12262	Cul3;Pbx1;Camk2d;Cdk1;Lsm11;Rad51b	0.0114	0.0326	GOBP	mmu-miR-192-5p
GO:0040014_regulation of multicellular organism growth	6	90	261	12262	Celf1;Pik3ca;Sgip1;Smo;Igf2;Tshr	0.0161	0.0329	GOBP	mmu-miR-192-5p
mmu04910_Insulin_signaling_pathway	25	140	777	8275	Eif4e2;Akt3;Ptpn1;Ppp1r3d;Pik3ca;Prkag2;Mapk10;Prkab1;Braf;Calm3;Prkar2a;Map2k2;Gck;Slc2a4;Crk;Calm1;Calml3;Prkaa1;Socs1;Pdpk1;Sos1;Ppp1r3c;Sorbs1;Araf;Phka1	0.0043	0.0332	KEGG	mmu-miR-345-5p
GO:0032922_circadian regulation of gene expression	5	66	261	12262	Hnrnpu;Top1;Gfpt1;Rora;Ppara	0.017	0.0333	GOBP	mmu-miR-192-5p
GO:0055092_sterol homeostasis	5	86	240	12262	Scarb1;Rora;Med13;G6pc;Pla2g10	0.0322	0.0341	GOBP	mmu-miR-21a-5p

GO:0032606_type I interferon production	5	85	240	12262	Tlr4;Gbp4;Azi2;Zbtb20;Chuk	0.0309	0.0341	GOBP	mmu-miR-21a-5p
GO:0042632_cholesterol homeostasis	5	85	240	12262	Scarb1;Rora;Med13;G6pc;Pla2g10	0.0309	0.0341	GOBP	mmu-miR-21a-5p
mmu05215_Prostate_cancer	22	97	768	8275	Creb1;E2f1;Pik3r3;Pik3cd;Pdgfra;Braf;Cdkn1b;Igf1r;Ccnd1;Cdk2;Egfr;Nfkbia;E2f3;Pik3r1;Etv5;Gsk3b;Erg;Hsp90ab1;Sos1;Pdgfrb;Pten;Ikbkg	0.0005	0.035	KEGG	mmu-miR-150-5p
mmu05212_Pancreatic_cancer	16	75	777	8275	Akt3;E2f1;Pik3ca;Tgfbr1;Casp9;Cdk6;Mapk10;Braf;Bax;Ccnd1;Tgfb3;E2f3;Cdkn1a;Smad2;Araf;Ikbkg	0.0047	0.0351	KEGG	mmu-miR-345-5p
GO:0034109_homotypic cell-cell adhesion	5	68	261	12262	Slc7a11;Ceacam1;Ubash3b;Cxadr;Prkg1	0.0189	0.0354	GOBP	mmu-miR-192-5p
mmu05223_Non-small_cell_lung_cancer	6	66	153	8275	Pik3ca;Nras;E2f2;Braf;Prkcb;Pik3r1	0.0022	0.0365	KEGG	mmu-miR-192-5p
GO:2001021_negative regulation of response to DNA damage stimulus	5	70	261	12262	Trim32;3110062M04Rik;Mb21d1;Ercc4;Ppp1r10	0.021	0.0378	GOBP	mmu-miR-192-5p
GO:0048525_negative regulation of viral process	6	97	261	12262	Trim32;Tardbp;Ceacam1;Pou2f3;Rsad2;Eif2ak2	0.022	0.0381	GOBP	mmu-miR-192-5p
mmu04722_Neurotrophin_signaling_pathway	22	121	777	8275	Bcl2;Mapkapk2;Akt3;Pik3ca;Mapk10;Braf;Calm3;Bax;Map2k7;Foxo3;Map2k2;Camk2b;Crk;Ngfr;Arhgdia;Psen1;Calm1;Calml3;Ntrk2;Pdpk1;Sos1;Camk2a	0.0058	0.0382	KEGG	mmu-miR-345-5p
mmu04012_ErbB_signaling_pathway	17	84	777	8275	Erbb4;Akt3;Src;Pik3ca;Mapk10;Braf;Map2k7;Nrg1;Map2k2;Camk2b;Map2k4;Crk;Cdkn1a;Sos1;Hbegf;Camk2a;Araf	0.0058	0.0382	KEGG	mmu-miR-345-5p
mmu05410_Hypertrophic_cardiomyopathy_(HCM)	17	84	777	8275	Des;Tpm3;Tpm2;Prkag2;Sgcb;Prkab1;Cacna2d4;Cacng7;Tpm4;Itga11;Tpm1;Sgca;Tgfb3;Sgcg;Prkaa1;Cacnb3;Emd	0.0058	0.0382	KEGG	mmu-miR-345-5p
mmu04728_Dopaminergic_synapse	24	135	777	8275	Creb1;Kcnj9;Akt3;Ppp2r2c;Mapk10;Creb3l2;Gng12;Itpr2;Calm3;G	0.0053	0.0382	KEGG	mmu-miR-345-5p

					nao1;Kif5a;Camk2b;Ppp2r3c;Calm1;Ppp2r5c;Calml3;Gng2;Ppp2r2a;Kcnj6;Atf6b;Ppp2r5d;Camk2a;Plcb3;Slc18a2				
mmu05167_Kaposi_sarcoma-associated_herpesvirus_infection	34	217	777	8275	Creb1;Mapkapk2;Akt3;E2f1;Src;Pik3ca;Ppp3r2;Casp9;Cdk6;Mapk10;Gng12;Bid;Itpr2;Calm3;Zfp36;Bax;Ccnd1;Map2k7;Ccr4;Map2k2;Ppp3r1;Map2k4;Pik3cg;Calm1;Calml3;E2f3;Il6st;Gng2;Atg14;Ifnar2;Rcan1;Cdkn1a;H2-T24;Ikbkg	0.0063	0.0403	KEGG	mmu-miR-345-5p
mmu04115_p53_signaling_pathway	15	71	777	8275	Bcl2;Steap3;Casp9;Cdk6;Serpine1;Bid;Ccne1;Bax;Ccnd1;Ei24;Perp;Rrm2;Cdkn1a;Pmaip1;Siah1b	0.0066	0.0411	KEGG	mmu-miR-345-5p
GO:0090174_organelle membrane fusion	6	100	261	12262	Vps39;Mfn1;Gnai3;Syt9;Sept8;Stx8	0.0249	0.0413	GOBP	mmu-miR-192-5p
GO:0010822_positive regulation of mitochondrion organization	5	74	261	12262	Mfn1;Mul1;Smurf1;Ddhd1;Pmaip1	0.0257	0.0413	GOBP	mmu-miR-192-5p
mmu04215_Apoptosis	9	32	777	8275	Bcl2;Bcl2l11;Casp9;Mapk10;Bid;Bax;Ngfr;Birc5;Pmaip1	0.0072	0.0414	KEGG	mmu-miR-345-5p
mmu04371_Apelin_signaling_pathway	24	139	777	8275	Hdac4;Akt3;Jag1;Tgfbr1;Prkag2;Prkab1;Serpine1;Gng12;Itpr2;Calm3;Mef2a;Ccnd1;Mras;Tfam;Map2k2;Adcy3;Pik3cg;Calm1;Calml3;Gng2;Prkaa1;Prkce;Smad2;Plcb3	0.0072	0.0414	KEGG	mmu-miR-345-5p
mmu04010_MAPK_signaling_pathway	43	294	777	8275	Erbb4;Mapkapk2;Elk4;Akt3;Lamtor3;Tgfbr1;Ppp3r2;Epha2;Mapk10;Braf;Gng12;Cacna2d4;Fgf23;Cacng7;Igf1r;Arrb1;Igf2;Map2k7;Mras;Map2k2;Kitl;Ptprr;Ppp3r1;Map2k4;Crk;Ngfr;Tgfb3;Ntrk2;Rasgrf2;Cacna1i;Mapk8ip2;Cacnb3;Map3k13;Efna5;Sos1;Ppm1b;Map3k8;Map3k2;Fgf1;Pdgfrb;Araf;I	0.0071	0.0414	KEGG	mmu-miR-345-5p

					kbkg;Fgf16				
GO:0010833_telomere maintenance via telomere lengthening	5	76	261	12262	Hnrnpu;Nek2;Map2k7;Atm;Ercc4	0.0282	0.0415	GOBP	mmu-miR-192-5p
GO:0032729_positive regulation of interferon-gamma production	5	77	261	12262	Abl2;Il21;Nras;Havcr2;Tnfrsf13c	0.0295	0.0415	GOBP	mmu-miR-192-5p
GO:1900182_positive regulation of protein localization to nucleus	5	75	261	12262	Tardbp;Smo;Cdk1;Pik3r1;Glis2	0.0269	0.0415	GOBP	mmu-miR-192-5p
GO:0014855_striated muscle cell proliferation	5	77	261	12262	Erbb4;Yap1;Cdk1;Jarid2;Cxadr	0.0295	0.0415	GOBP	mmu-miR-192-5p
mmu04550_Signaling_pathways_regulating_pluripotency_of_stem_cells	27	137	768	8275	Fzd5;Lefty2;Pax6;Skil;Sox2;Smad9;Pik3r3;Id3;Pik3cd;Fzd10;Igf1r;Kat6a;Smad3;Inhbe;Otx1;Wnt9a;Dvl2;Hoxb1;Fzd2;Pik3r1;Lifr;Acvr1b;Gsk3b;Pou5f1;Apc;Pcgf5;Dusp9	0.0008	0.042	KEGG	mmu-miR-150-5p
mmu04725_Cholinergic_synapse	7	113	153	8275	Kcnq2;Pik3ca;Nras;Gnai3;Camk2d;Prkcb;Pik3r1	0.0072	0.042	KEGG	mmu-miR-192-5p
mmu05225_Hepatocellular_carcinoma	9	171	153	8275	Pik3ca;Nras;E2f2;Braf;Prkcb;Igf2;Tcf7;Pik3r1;Frat1	0.0068	0.042	KEGG	mmu-miR-192-5p
mmu05213_Endometrial_cancer	5	58	153	8275	Pik3ca;Nras;Braf;Tcf7;Pik3r1	0.0062	0.042	KEGG	mmu-miR-192-5p
mmu04931_Insulin_resistance	7	109	153	8275	Prkag3;Pik3ca;Prkab2;Gfpt1;Prkcb;Pik3r1;Ppara	0.006	0.042	KEGG	mmu-miR-192-5p
mmu04068_FoxO_signaling_pathway	8	132	153	8275	Prkag3;Pik3ca;Prkab2;Nras;Braf;Atm;Agap2;Pik3r1	0.0048	0.042	KEGG	mmu-miR-192-5p
mmu04210_Apoptosis	8	136	153	8275	Pik3ca;Nras;Atm;Map3k14;Pik3r1;Csf2rb;Pmaip1;Ctsf	0.0057	0.042	KEGG	mmu-miR-192-5p
mmu05205_Proteoglycans_in_cancer	10	204	153	8275	Erbb4;Pik3ca;Nras;Camk2d;Smo;Braf;Prkcb;Igf2;Arhgef12;Pik3r1	0.0072	0.042	KEGG	mmu-miR-192-5p
mmu04923_Regulation_of_lipolysis_in_adipocytes	5	55	153	8275	Pik3ca;Gnai3;Tshr;Pik3r1;Prkg1	0.005	0.042	KEGG	mmu-miR-192-5p
mmu04730_Long-term_depression	5	61	153	8275	Nras;Gnai3;Braf;Prkcb;Prkg1	0.0075	0.042	KEGG	mmu-miR-192-5p
mmu04213_Longevity_regulating_pathway	5	62	153	8275	Prkag3;Pik3ca;Prkab2;Nras;Pik3r1	0.008	0.042	KEGG	mmu-miR-192-5p

mmu05210_Colorectal_cancer	6	88	153	8275	Pik3ca;Nras;Braf;Tcf7;Pik3r1;Pmaip1	0.0081	0.042	KEGG	mmu-miR-192-5p
mmu04068_FoxO_signaling_pathway	23	132	777	8275	Akt3;Bcl2l11;Tnfsf10;Pik3ca;Tgfbr1;Prkag2;Mapk10;Prkab1;Braf;Igf1r;Homer2;Ccnd1;Foxo3;Map2k2;S1pr4;Slc2a4;Tgfb3;Prkaa1;Pdpk1;Cdkn1a;Sos1;Smad2;Araf	0.0076	0.0426	KEGG	mmu-miR-345-5p
mmu04310_Wnt_signaling_pathway	25	148	777	8275	Wnt2b;Dkk2;Invs;Ppp3r2;Cer1;Fzd1;Mapk10;Fzd9;Wnt2;Prickle2;Ccnd1;Apc2;Camk2b;Ppp3r1;Fbxw11;Tcf7;Wnt9a;Psen1;Wnt5a;Fzd3;Wnt1;Camk2a;Plcb3;Frat1;Siah1b	0.0078	0.0426	KEGG	mmu-miR-345-5p
GO:0043525_positive regulation of neuron apoptotic process	5	79	261	12262	Epha7;Map2k7;Atm;Map2k4;Pmaip1	0.0323	0.0428	GOBP	mmu-miR-192-5p
GO:0050805_negative regulation of synaptic transmission	5	79	261	12262	Braf;S1pr2;Arf1;Pcdh17;Sorcs3	0.0323	0.0428	GOBP	mmu-miR-192-5p
mmu04130_SNARE_interactions_in_vesicular_transport	9	33	777	8275	Vamp4;Stx16;Stx17;Bet1l;Ykt6;Stx8;Gosr1;Gosr2;Vti1a	0.0085	0.0453	KEGG	mmu-miR-345-5p
mmu04310_Wnt_signaling_pathway	28	148	768	8275	Fzd5;Vangl2;Csnk2a1;Nfatc2;Tbl1xr1;Invs;Fzd10;Ccnd2;Ccnd1;Dkk4;Smad3;Rhoa;Ppp3r1;Wnt9a;Dvl2;Sost;Fzd2;Prkca;Rock2;Daam1;Nfatc4;Gsk3b;Daam2;Apc;Camk2a;Csnk1a1;Nfatc1;Lrp5	0.0011	0.0462	KEGG	mmu-miR-150-5p
mmu04720_Long-term_potentiation	14	67	777	8275	Grin1;Ppp3r2;Braf;Itpr2;Calm3;Grm5;Map2k2;Camk2b;Ppp3r1;Calm1;Calml3;Camk2a;Plcb3;Araf	0.0092	0.0479	KEGG	mmu-miR-345-5p

Supplementary Table 4

Name	Hits	Pop Hits	List Total	Pop Total	Genes	Pvalue	adjusted Pvalue (BH)	Ontology	MicroRNA
mmu04360_Axon_guidance	45	175	814	8275	Sema4c;Enah;Plxna2;Pdk1;Pak6;Nfatc2;Pik3ca;Efna1;Efna3;Bmpr1b;Pik3r3;Epha8;Cdc42;Gnai1;Shh;Dpysl5;Ablim2;Slit2;Ssh1;Sema4f;Plxna1;Srgap3;Efnb2;Trpc6;Arhgef12;Trpc1;Ryk;Sema3f;Fyn;Plxnc1;Limk2;Prkca;Ptch1;Ppp3cb;Camk2g;Fzd3;Rac2;Mapk1;Ephb3;Pak2;Epha3;Efna5;Sema4g;Ablim1;Pak3	0	0	KEGG	mmu-let-7d-5p
mmu04130_SNARE_interactions_in_vesicular_transport	16	33	814	8275	Vamp4;Sec22b;Stx17;Vamp3;Stx2;Vamp5;Vamp1;Bet1l;Stx11;Stx7;Ykt6;Stx8;Bnip1;Stx5a;Stx3;Vti1a	0	0	KEGG	mmu-let-7d-5p
mmu04310_Wnt_signaling_pathway	33	148	814	8275	Csnk2a1;Nfatc2;Vangl1;Lef1;Dvl1;Fzd1;Mapk10;Tcf7l1;Ccnd2;Prkcb;Prkaca;Nkd1;Ctnnb1;Apc2;Fbxw11;Skp1a;Tcf7;Wnt9a;Nlk;Wnt3;Prkca;Psen1;Ppp3cb;Camk2g;Chd8;Fzd3;Rac2;Csnk1a1;Nfatc1;Lrp5;Dkk1;Sfrp5;Btrc	0.0001	0.0048	KEGG	mmu-let-7d-5p
mmu04340_Hedgehog_signaling_pathway	16	44	814	8275	Cul3;Shh;Adrbk2;Smurf1;Ccnd2;Prkaca;Cdon;Csnk1g1;Fbxw11;Kif3a;Ptch1;Dhh;Csnk1a1;Adrbk1;Btrc;Sufu	0.0001	0.0048	KEGG	mmu-let-7d-5p
mmu04014_Ras_signaling_pathway	45	233	814	8275	Ralb;Abl2;Fasl;Akt3;Pak6;Shc4;Pik3ca;Efna1;Efna3;Pik3r3;Cdc42;Gnb1;Mapk10;Tgfa;Pla2g4c;Rasgrp4;Gab2;Prkcb;Fgf15;Fgfr1;Gab1;Prkaca;Calml4;Mras;Shc2;Igf1;Rab5b;Ksr1;Nf1;Prkca;Gng4;Ntrk2;Fgf9;Angpt1;Rac2;Mapk1;Pak2;Ets2;Mllt4;Rasal3;Efna5;Elk1;Ikbkg;Fgf16;Pak3	0.0001	0.0048	KEGG	mmu-let-7d-5p
mmu04370_VEGF_signaling_pathway	17	58	814	8275	Ptgs2;Akt3;Nfatc2;Pik3ca;Pik3r3;Cdc42;Nos3;Pxn;Pla2g4c;Prkcb;Shc2;Prkca;Ppp3cb;Rac2;Mapk1;Mapk14;Mapk13	0.0003	0.0121	KEGG	mmu-let-7d-5p
mmu04152_AMPK_signaling_pathway	27	126	814	8275	Creb1;Cab39;Pfkfb2;Akt3;Pfkfb3;Tsc1;Hnf4a;Pik3ca;Rab2a;Lepr;Pik3r3;Ppp2r2c;Ppargc1a;Eef2k;Elavl1;Pfkfb4;Foxo3;Pfkl;Stk11;Igf1;Slc2a4;Strada;Pp	0.0006	0.0182	KEGG	mmu-let-7d-5p

					p2r3c;Pfkp;Cab39l;Scd3;Scd1				
mmu05224_Breast_cancer	30	147	814	8275	Akt3;Shc4;Ncoa3;Pik3ca;Lef1;Pik3r3;E2f2;Dvl1;Cdk6;Fzd1;Brca2;Braf;Tcf7l1;Fgf15;Fgfr1;Ctnnb1;Shc2;Apc2;Igf1;Tcf7;Wnt9a;Wnt3;Fgf9;Fzd3;Sp1;Mapk1;Csnk1a1;Lrp5;Pten;Fgf16	0.0006	0.0182	KEGG	mmu-let-7d-5p
mmu04012_ErbB_signaling_pathway	20	84	814	8275	Erbb4;Abl2;Akt3;Pak6;Shc4;Pik3ca;Pik3r3;Mapk10;Braf;Tgfa;Prkcb;Nrg1;Gab1;Shc2;Prkca;Camk2g;Mapk1;Pak2;Elk1;Pak3	0.0009	0.0198	KEGG	mmu-let-7d-5p
mmu04550_Signaling_pathways_regulating_pluripotency_of_stem_cells	28	137	814	8275	Akt3;Bmi1;Pik3ca;Smad9;Bmpr1b;Pik3r3;Dvl1;Fzd1;Hnf1a;Fgfr1;Smad1;Acvr2b;Ctnnb1;Nodal;Apc2;Igf1;Lif;Wnt9a;Hoxb1;Wnt3;Esrrb;Inhba;Fzd3;Lifr;Acvr1b;Mapk1;Mapk14;Mapk13	0.0009	0.0198	KEGG	mmu-let-7d-5p
mmu04071_Sphingolipid_signaling_pathway	26	122	814	8275	Akt3;9130409I23Rik;Pik3ca;Adora3;Sgms2;Pik3r3;Gnai1;Nos3;Ppp2r2c;Mapk10;Cers3;Gab2;Prkcb;Fyn;Sgpl1;Prkca;Ppp2r3c;Sptlc2;S1pr3;Rac2;Mapk1;Mapk14;Mapk13;Acer1;Gnaq;Pten	0.0008	0.0198	KEGG	mmu-let-7d-5p
mmu04664_Fc_epsilon_RI_signaling_pathway	17	68	814	8275	Akt3;Vav2;Pik3ca;Lyn;Pik3r3;Mapk10;Pla2g4c;Gab2;Fyn;Il13;Il5;Prkca;Syk;Rac2;Mapk1;Mapk14;Mapk13	0.0014	0.0282	KEGG	mmu-let-7d-5p
mmu04010_MAPK_signaling_pathway	48	294	814	8275	Erbb4;Cacna1e;Fasl;Akt3;Cacnb4;Zak;Il1a;Il1b;Efna1;Efna3;Mknk1;Cdc42;Mapk10;Taok3;Braf;Tgfa;Pla2g4c;Rasgrp4;Prkcb;Fgf15;Fgfr1;Prkaca;Mras;Cacna2d2;Tab2;Igf1;Dusp6;Nlk;Nf1;Prkca;Tgfb3;Ntrk2;Flnb;Ppp3cb;Fgf9;Angpt1;Rac2;Mapk1;Pak2;Mapk14;Mapk13;Srf;Efna5;Map3k2;Nfatc1;Elk1;Ikbkg;Fgf16	0.0017	0.0316	KEGG	mmu-let-7d-5p
mmu04722_Neurotrophin_signaling_pathway	24	121	814	8275	Fasl;Akt3;Shc4;Pik3ca;Pik3r3;Cdc42;Trp73;Mapk10;Sh2b3;Braf;Irak2;Nfkbib;Gab1;Calml4;Foxo3;Shc2;Prdm4;Psen1;Ntrk2;Camk2g;Prkcd;Mapk1;Mapk14;Mapk13	0.0027	0.0357	KEGG	mmu-let-7d-5p
mmu01521_EGFR_tyrosine_kinase_inhibitor_resistance	18	80	814	8275	Eif4e2;Akt3;Shc4;Pik3ca;Il6ra;Pik3r3;Braf;Tgfa;Prkcb;Nrg1;Gab1;Foxo3;Shc2;Igf1;Nf1;Prkca;Mapk1;Pten	0.0028	0.0357	KEGG	mmu-let-7d-5p
mmu05225_Hepatocellular_carcinoma	31	171	814	8275	Akt3;Shc4;Pik3ca;Lef1;Pik3r3;E2f2;Dvl1;Cdk6;Fzd1;Braf;Tcf7l1;Tgfa;Prkcb;Gab1;Ctnnb1;Shc2;Apc	0.0026	0.0357	KEGG	mmu-let-7d-5p

					2;Tcf7;Wnt9a;Wnt3;Prkca;Tgfb3;Fzd3;Smarcd1;Mapk1;Txnrd2;Arid1b;Csnk1a1;Lrp5;Pten;Elk1				
mmu04510_Focal_adhesion	35	199	814	8275	Col4a3;Ppp1r12b;Lamc1;Akt3;Itga8;Vav2;Itgav;Pak6;Shc4;Pik3ca;Pik3r3;Cdc42;Mapk10;Pxn;Ppp1cc;Braf;Ccnd2;Prkcb;Birc3;Tln2;Itga9;Ctnnb1;Fyn;Shc2;Igf1;Prkca;Arhgap5;Flnb;Rac2;Mapk1;Pak2;Pten;Elk1;Xiap;Pak3	0.0022	0.0357	KEGG	mmu-let-7d-5p
mmu04916_Melanogenesis	21	100	814	8275	Creb1;Lef1;Dvl1;Fzd1;Gnai1;Tcf7l1;Tyr;Prkcb;Prkaca;Gnao1;Calml4;Ctnnb1;Tcf7;Wnt9a;Wnt3;Prkca;Edn1;Camk2g;Fzd3;Mapk1;Gnaq	0.0027	0.0357	KEGG	mmu-let-7d-5p
mmu04520_Adherens_junction	17	72	814	8275	Nectin4;Ptprj;Csnk2a1;Lef1;Cdc42;Tcf7l1;Fgfr1;Ctnnb1;Fyn;Ptprb;Tcf7;Nlk;Baiap2;Rac2;Mapk1;Mllt4;Fer	0.0023	0.0357	KEGG	mmu-let-7d-5p
mmu05205_Proteoglycans_in_cancer	35	204	814	8275	Erbb4;Ppp1r12b;Fasl;Akt3;Vav2;Hoxd10;Itgav;Pik3ca;Tlr4;Pik3r3;Cdc42;Fzd1;Shh;Pxn;Ppp1cc;Braf;Prkcb;Fgfr1;Gab1;Prkaca;Arhgef12;Mras;Ctnnb1;Igf1;Wnt9a;Wnt3;Prkca;Ptch1;Flnb;Camk2g;Fzd3;Mapk1;Mapk14;Mapk13;Elk1	0.0032	0.0387	KEGG	mmu-let-7d-5p
mmu04140_Autophagy	12	130	232	8275	Rab7b;Tsc1;Rragd;Wipi2;Rras2;Map2k2;Mapk9;Gabarap;Ern1;Atg2b;Mapk8;Mapk1	0.0007	0.0388	KEGG	mmu-miR-142a-3p
mmu04010_MAPK_signaling_pathway	20	294	232	8275	Traf2;Bdnf;Rasgrp1;Stk4;Cdc42;Cacna1c;Arrb1;Rras2;Cacna1a;Map2k2;Igf1;Mapk9;Taok1;Dusp3;Ntrk2;Mapk8;Cacna1i;Mapk1;Ppm1b;Fgf16	0.0007	0.0388	KEGG	mmu-miR-142a-3p
GO:0051057_positive regulation of small GTPase mediated signal transduction	10	70	408	12262	Rasgrp1;Arrb1;Nrg1;Cdon;Arpp19;Igf1;Rtn4;Abra;Gm5127;Gpr174	0.0003	0.0398	GOBP	mmu-miR-142a-3p
GO:0046579_positive regulation of Ras protein signal transduction	9	63	408	12262	Rasgrp1;Arrb1;Nrg1;Arpp19;Igf1;Rtn4;Abra;Gm5127;Gpr174	0.0005	0.0398	GOBP	mmu-miR-142a-3p
mmu04625_C-type_lectin_receptor_signaling_pathway	22	112	814	8275	Ptgs2;Akt3;Il1b;Nfatc2;Pik3ca;Pik3r3;Mapk10;Lsp1;Ccl22;Arhgef12;Calml4;Mras;Egr2;Ksr1;Syk;Pp p3cb;Prkcd;Mapk1;Mapk14;Mapk13;Nfatc1;Ikbkg	0.0043	0.0419	KEGG	mmu-let-7d-5p
mmu04070_Phosphatidylinositol_signaling_system	20	98	814	8275	Inpp4a;Plcd4;Dgkd;Pik3c2b;Inpp5e;Impa1;Pik3ca;Pik3r3;Dgki;Pik3c2a;Prkcb;Cdipt;Calml4;Inpp5j;Pip4k2b;Prkca;Synj2;Pten;Pi4k2a;Mtmr1	0.0044	0.0419	KEGG	mmu-let-7d-5p

mmu04066_HIF-1_signaling_pathway	21	105	814	8275	Eif4e2;Akt3;Pfkfb3;Pdk1;Pik3ca;Il6ra;Tlr4;Mknk1;Pik3r3;Nppa;Nos3;Hk2;Ldha;Prkcb;Pfkl;Igf1;Prkca;Edn1;Camk2g;Angpt1;Mapk1	0.0044	0.0419	KEGG	mmu-let-7d-5p
mmu04120_Ubiquitin_mediated_proteolysis	26	139	814	8275	Cul3;Itch;Ube2j1;Ube2j2;Ube2k;Rchy1;Smurf1;Ube2h;Herc3;Ube2m;Sae1;Birc3;Ube4a;Cdc34;Fbxw11;Ube2b;Skp1a;Ercc8;Mgrn1;Ube2i;Cdc23;Nedd4l;Prpf19;Btrc;Xiap;Mid1	0.0037	0.0419	KEGG	mmu-let-7d-5p
mmu05214_Glioma	16	71	814	8275	Akt3;Shc4;Pik3ca;Pik3r3;E2f2;Cdk6;Braf;Tgfa;Prkcb;Calml4;Shc2;Igf1;Prkca;Camk2g;Mapk1;Pten	0.0045	0.0419	KEGG	mmu-let-7d-5p
mmu05215_Prostate_cancer	20	97	814	8275	Creb1;Akt3;Pik3ca;Lef1;Pik3r3;E2f2;Braf;Tcf7l1;Tgfa;Fgfr1;Ctnnb1;Igf1;Tcf7;Mapk1;Etv5;Tmprss2;Zeb1;Pten;Ikbkg;Ar	0.004	0.0419	KEGG	mmu-let-7d-5p
mmu04728_Dopaminergic_synapse	25	135	814	8275	Creb1;Kcnj9;Akt3;Gnb1;Gnai1;Ppp2r2c;Clock;Mapk10;Ppp1cc;Prkcb;Prkaca;Gnao1;Gria4;Calml4;Ddc;Ppp1r1b;Prkca;Ppp2r3c;Gng4;Ppp3cb;Camk2g;Mapk14;Mapk13;Gnaq;Gria3	0.0049	0.0439	KEGG	mmu-let-7d-5p
mmu04933_AGE-RAGE_signaling_pathway_in_diabetic_complications	20	100	814	8275	Plcd4;Col4a3;Akt3;Il1a;Il1b;Pik3ca;Pik3r3;Cdc42;Nos3;Mapk10;Prkcb;Prkca;Tgfb3;Edn1;Prkcd;Mapk1;Mapk14;Mapk13;Pim1;Nfatc1	0.0053	0.0442	KEGG	mmu-let-7d-5p
mmu04724_Glutamatergic_synapse	22	114	814	8275	Gls;Glul;Gnb1;Gnai1;Adrbk2;Pla2g4c;Shank1;Grm5;Prkcb;Prkaca;Gnao1;Gria4;Trpc1;Grm1;Prkca;Gng4;Ppp3cb;Mapk1;Dlgap1;Adrbk1;Gnaq;Gria3	0.0052	0.0442	KEGG	mmu-let-7d-5p
mmu04921_Oxytocin_signaling_pathway	27	153	814	8275	Ppp1r12b;Rgs2;Ptgs2;Kcnj9;Camk1d;Cacnb4;Nfatc2;Gnai1;Nos3;Ppp1cc;Camk1;Pla2g4c;Eef2k;Prkcb;Prkaca;Gnao1;Gucy1a2;Calml4;Cacna2d2;Trpm2;Prkca;Ppp3cb;Camk2g;Mapk1;Nfatc1;Gnaq;Elk1	0.0062	0.0462	KEGG	mmu-let-7d-5p
mmu04660_T_cell_receptor_signaling_pathway	20	101	814	8275	Icos;Ptprc;Akt3;Vav2;Pak6;Nfatc2;Pik3ca;Pik3r3;Cdc42;Nfkbib;Fyn;Il5;Ppp3cb;Mapk1;Pak2;Mapk14;Mapk13;Nfatc1;Ikbkg;Pak3	0.0058	0.0462	KEGG	mmu-let-7d-5p
mmu04150_mTOR_signaling_pathway	27	153	814	8275	Cab39;Eif4e2;Rnf152;Akt3;Tsc1;Pik3ca;Fnip2;Pik3r3;Dvl1;Fzd1;Braf;Atp6v1b1;Lamtor1;Prkcb;Stk11;Igf1;Fnip1;Wnt9a;Wnt3;Strada;Prkca;Cab39l;Fzd3;Deptor;Mapk1;Lrp5;Pten	0.0062	0.0462	KEGG	mmu-let-7d-5p
mmu04062_Chemokine_signaling_pathway	33	199	814	8275	Akt3;Vav2;Shc4;Pik3ca;Lyn;Pik3r3;Fgr;Cdc42;Gnb1;LOC100041504;Gnai1;Cxcl9;Adrbk2;Pxn;Braf;	0.0063	0.0462	KEGG	mmu-let-7d-5p

					Nfkbib;Prkcb;Prkaca;Ccl22;Ccr9;Ccr1l1;Foxo3;Shc2;Ccl9;Ccl3;Ccr10;Gng4;Prkcd;Rac2;Mapk1;Adrbk1;Grk5;Ikbkg				
mmu04730_Long-term_depression	14	61	814	8275	Lyn;Gnai1;Braf;Pla2g4c;Prkcb;Gnao1;Gucy1a2;Grm1;Igf1;Crhr1;Prkca;Mapk1;Gnaq;Gria3	0.0066	0.047	KEGG	mmu-let-7d-5p
mmu05163_Human_cytomegalovirus_infection	40	256	814	8275	Creb1;Ptgs2;Fasl;Akt3;Tsc1;Itgav;Il1b;Nfatc2;Pik3ca;Il6ra;Pik3r3;E2f2;Gnb1;Cdk6;Gnai1;Pxn;Prkcb;Prkaca;Gnao1;Arhgef12;Il10ra;Calml4;Ctnnb1;Ccr1l1;Ccl3;Prkca;Gng4;Ripk1;Ppp3cb;Ptger2;Rac2;Sp1;Mapk1;Mapk14;Mapk13;Tapbp;Nfatc1;Gnaq;Elk1;Ikbkg	0.007	0.0471	KEGG	mmu-let-7d-5p
mmu05212_Pancreatic_cancer	16	75	814	8275	Ralb;Akt3;Pik3ca;Pik3r3;E2f2;Cdc42;Cdk6;Mapk10;Brca2;Braf;Tgfa;Tgfb3;Rac2;Mapk1;Arhgef6;Ikbkg	0.007	0.0471	KEGG	mmu-let-7d-5p
GO:0055026_negative regulation of cardiac muscle tissue development	7	41	408	12262	Fzd7;Rgs2;Sox6;Cited2;Meis1;Tomm70a;Cxadr	0.0009	0.0477	GOBP	mmu-miR-142a-3p

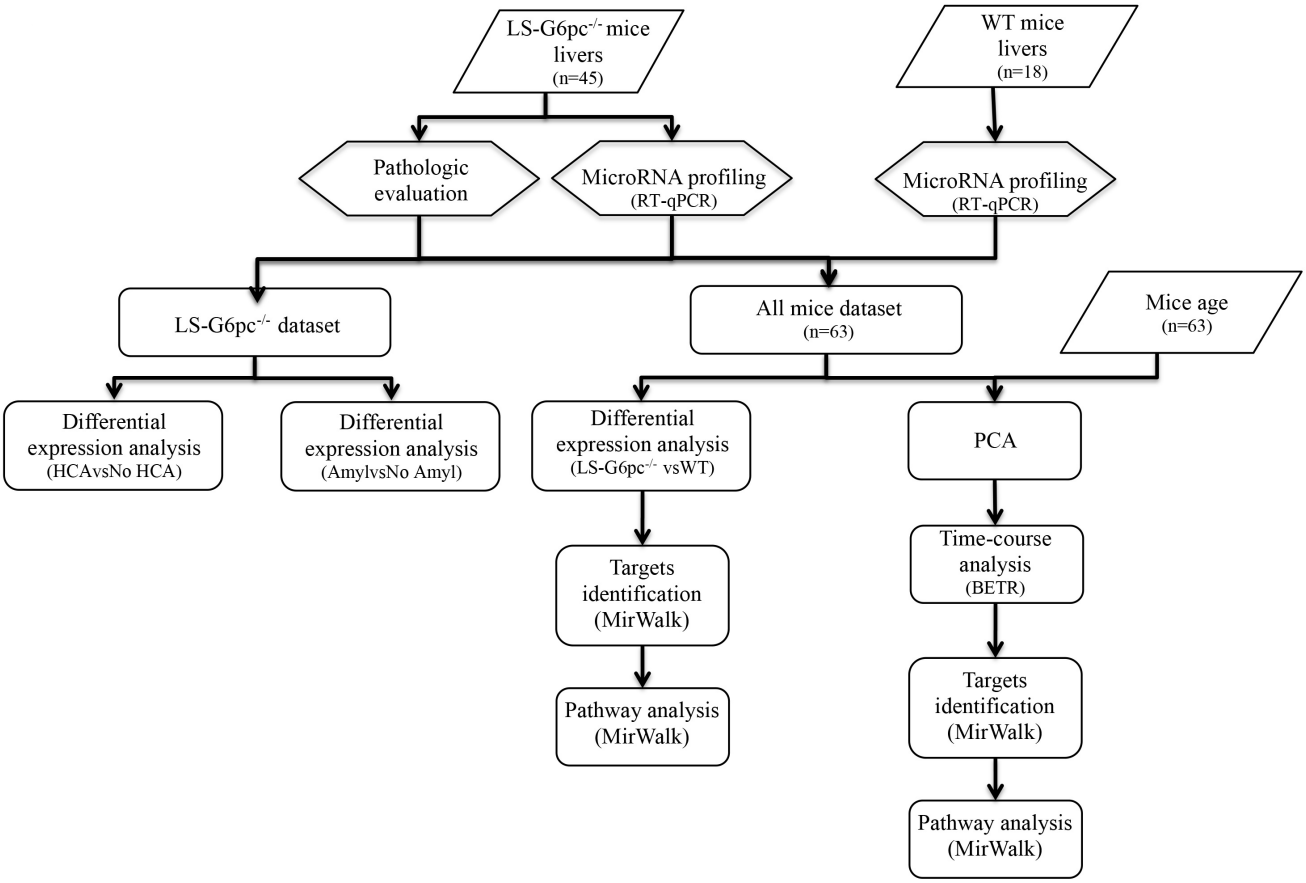

Fig. S1. Schematic representation of the whole bioinformatic strategy used in the study. The microRNA representation profile of 45 LS-G6pc$^{-/-}$ and 18 WT mouse plasma exosomes was measured by ViiA 7 RT-qPCR. Pathological evaluation of the livers assessed the presence of hepatic adenomas and/or amyloidosis within the entire set of mice samples. Differential expression analysis assessed any significant modulation of the Exo-miR between groups of LS-G6pc$^{-/-}$ and WT mice, LS-G6pc$^{-/-}$ mice characterized by the presence\absence of hepatic adenomas, or LS-G6pc$^{-/-}$ mice characterized by the presence/absence of amyloidosis. The representation profile of LS-G6pc$^{-/-}$ and WT mice over 6 distinct age groups was compared using BETR method. Analysis identified age-dependent modulated Exo-miR whose targets were identified using MirWalk tool. Pathway analysis on these targets identified the most significantly altered biological processes and pathways.

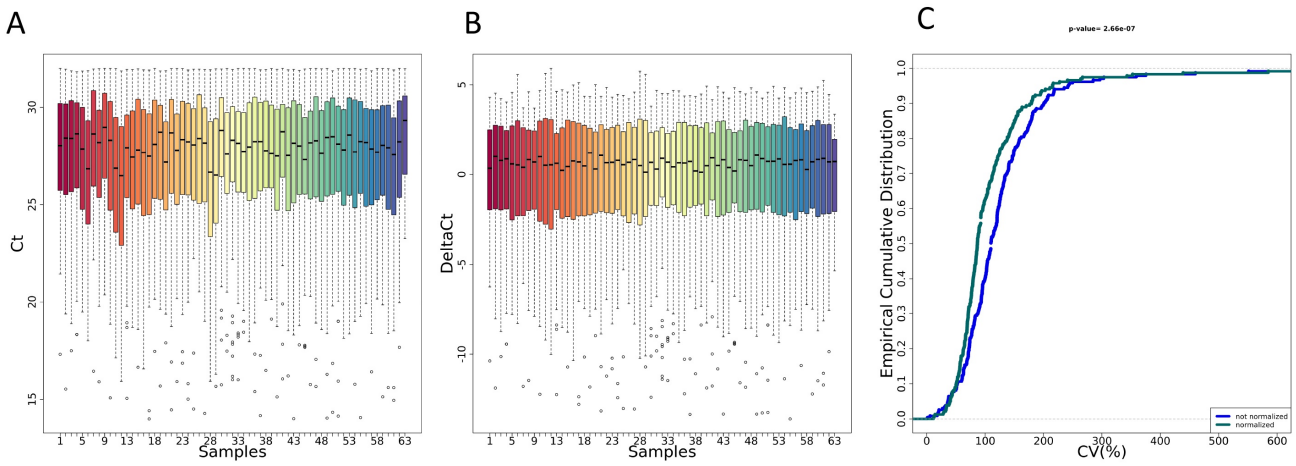

Fig. S2. Qualitative and quantitative assessment of the noise reduction for LS-G6pc$^{-/-}$ and WT mice data

The box plots reported in panels A and B show the distribution of Ct and delta Ct values for every samples before and after data normalization, respectively. The plot reported in panel C show the ECDFs (y axis) and the coefficient of variation (CV) for every samples before (blue line) and after (Green line) data normalization. Kolmogorov-Smirnov test assessed the significance of the separation between the curves and the p-value is reported on top of the plot. P-value lower than 0.05 is considered significant. Global mean was used to normalize the data.

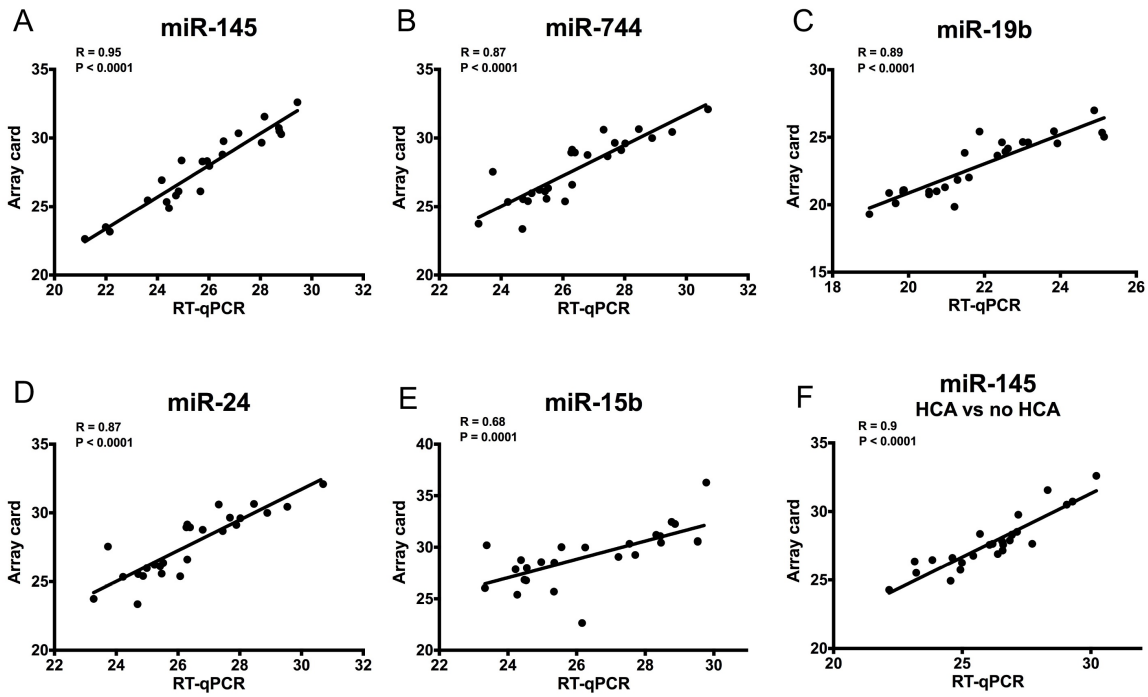

Fig. S3. Scatter plots of Ct values measured by RT-qPCR and Array card

A scatter plot showing correlation between the expression values measured by RT-qPCR and Array card on LS-G6pc$^{-/-}$ and WT mice samples is depicted for a selection of significant Exo-miR**.** Each point is the Ct value of a sample measured by RT-qPCR and Array card. Correlation is assessed by Pearson method. Linear regression line is superimposed to the points within each plot. Pearson correlation and p-value are reported in the top left side of the plots.

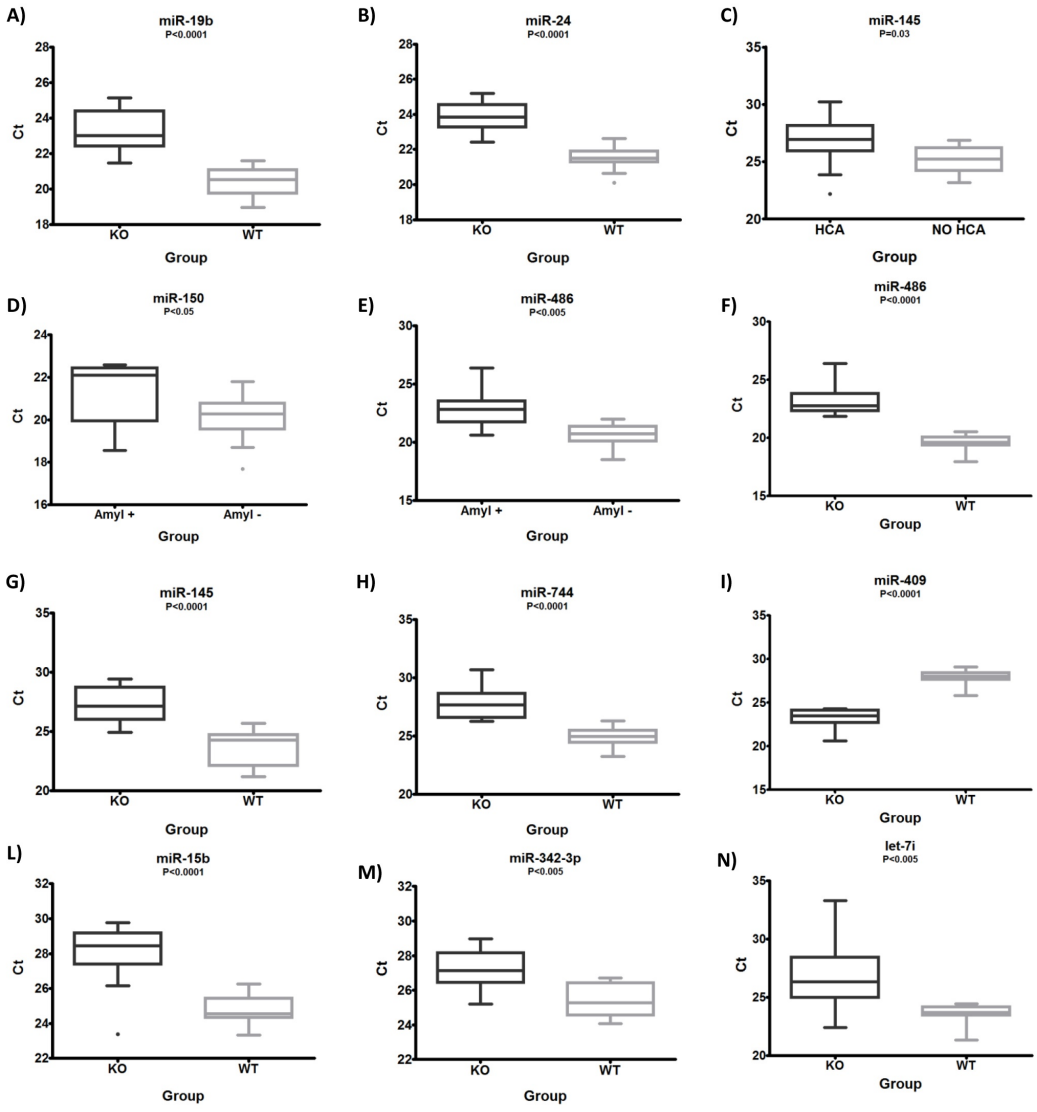

Fig. S4. Box plots of Ct values measured by RTqPCR between LS-G6pc$^{-/-}$ and WT mice; LS-G6pc$^{-/-}$ mice with and without amyloidosis; LS-G6pc$^{-/-}$ mice with and without adenoma.

Box-plots showing the differential expression between LS-G6pc$^{-/-}$ and WT mice, between LS-G6pc$^{-/-}$ mice with and without amyloidosis and between LS-G6pc$^{-/-}$ mice with and without adenoma are depicted for a selection of significant Exo-miR. Ct values were measured by RTqPCR. Statistical significance of the difference is assessed by unpaired t-test. P values and the name of the microRNA are reported on the top of each plot.

Table S1. Enrichment of GO biological processes and KEGG pathways in LS-G6pc$^{-/-}$ versus WT mice.

Click here to Download Table S1

Table S2. Enrichment of GO biological processes and KEGG pathways in LS-G6pc$^{-/-}$ mice with HCA versus LS-G6pc$^{-/-}$ mice without HCA.

Click here to Download Table S2

Table S3. Enrichment of GO biological processes and KEGG pathways LS-G6pc$^{-/-}$ mice with amyloidosis versus LS-G6pc$^{-/-}$ mice without amyloidosis.

Click here to Download Table S3

Table S4. Enrichment of GO biological processes and KEGG pathways in LS-G6pc$^{-/-}$ versus WT mice over time.

Click here to Download Table S4